agrochemicals

MDPI

Article

Differential Effects of *O*-Benzyl-Serine on Sulfur Metabolism, Photosynthesis, and Growth in Two Species of Weeds

Isabela de Carvalho Contesoto [1], Ana Paula Boromelo [1], Ana Paula da Silva Mendonça [1], Cinthia Martins Corbetta [1], Amanda Castro Comar [1], Marco Aurélio Schüler de Oliveira [2], Larissa Fonseca Tomazini [2], João Henrique Vieira de Almeida Junior [3], Marcelo Augusto Batista [3], Paulo Sérgio Alves Bueno [2], Caroline Barbeiro [4], Ana Paula Ferro [1,5], Wanderley Dantas dos Santos [1], Rodrigo Polimeni Constantin [1,5], Osvaldo Ferrarese-Filho [1,*] and Rogério Marchiosi [1,*]

[1] Laboratory of Plant Biochemistry, Department of Biochemistry, State University of Maringá, Maringá 87020-900, Brazil; isabelacontesoto@gmail.com (I.d.C.C.); boromeloanapaula@gmail.com (A.P.B.); silvamendoncaanapaula@gmail.com (A.P.d.S.M.); pg56294@uem.br (C.M.C.); amandacomar9@gmail.com (A.C.C.); apferro2@uem.br (A.P.F.); wdsantos@uem.br (W.D.d.S.); rpconstantin@uem.br (R.P.C.)

[2] Laboratory of Molecular Biology of Prokaryotes, Department of Biochemistry, State University of Maringá, Maringá 87020-900, Brazil; masoliveira2@uem.br (M.A.S.d.O.); larissa_tomazini@hotmail.com (L.F.T.); psabueno2@uem.br (P.S.A.B.)

[3] Department of Agronomy, State University of Maringá, Maringá 87020-900, Brazil; pg55476@uem.br (J.H.V.d.A.J.); mabatista@uem.br (M.A.B.)

[4] Laboratory of Seed and Seedling Physiology, Department of Biology, State University of Maringa, Maringá 87020-900, Brazil; cbarbeiro@uem.br

[5] Department of Biochemistry, Laboratory of Biological Oxidations, State University of Maringá, Maringá 87020-900, Brazil

* Correspondence: osferrarese@uem.br (O.F.-F.); rmarchiosi@uem.br (R.M.)

Abstract

Enzymes of the sulfur assimilation pathway represent promising candidates for selective herbicide development. This study investigated the effects of *O*-benzyl-serine (OBS), a newly identified inhibitor of *O*-acetylserine(thiol)-lyase (OAS-TL), on two C3 weed species, *Ipomoea grandifolia* and *Euphorbia heterophylla*. Plants were cultivated hydroponically for 12 days in the presence of OBS (0–500 µM). OBS inhibited root growth in both species in a dose-dependent manner, with *I. grandifolia* being more sensitive. OAS-TL activity decreased in the roots of *I. grandifolia* but increased in the leaves of *E. heterophylla*. Nutrient profiling revealed significant alterations in sulfur, magnesium, and calcium contents, associated with chlorosis and reduced root and leaf development. While photosynthetic performance appeared unaffected at the lowest OBS concentration tested (62.5 µM), higher doses drastically reduced leaf expansion, preventing further measurements. Given this marked decline in foliar development, it is reasonable to infer that the overall photosynthetic capacity of the plants was also negatively affected under severe OBS exposure. OBS also disrupted apical dominance, promoting lateral shoot formation. These findings demonstrate that OBS differentially affects sulfur metabolism and growth in a species- and organ-specific manner, supporting its potential as a prototype molecule for herbicides targeting novel biochemical pathways.

Keywords: axillary bud development; nutrient imbalance; enzyme activity modulation; chlorosis; phytohormonal disruption

Check for updates

Academic Editor: Yu Gao

Received: 17 October 2025
Revised: 12 December 2025
Accepted: 6 January 2026
Published: 9 January 2026

Copyright: © 2026 by the authors. Licensee MDPI, Basel, Switzerland. This article is an open access article distributed under the terms and conditions of the Creative Commons Attribution (CC BY) license.

1. Introduction

Fully established plants rely on photosynthesis as their primary energy source, and a wide range of components, including macro and micronutrients, are essential throughout their development to sustain their intricate metabolic machinery. The macronutrients required in larger quantities include nitrogen (N), potassium (K), calcium (Ca), magnesium (Mg), phosphorus (P), and sulfur (S), while the micronutrients, necessary in smaller amounts but equally critical, encompass iron (Fe), zinc (Zn), manganese (Mn), copper (Cu), boron (B), chlorine (Cl), molybdenum (Mo), and nickel (Ni) [1]. Each of these nutrients is required in varying quantities depending on the species, and even within individual plant tissues, nutrient demands can fluctuate significantly [2]. Furthermore, these nutrients serve as integral components of specific molecules and play indispensable roles in a multitude of metabolic processes. For instance, nitrogen is a fundamental constituent of amino acids, the building blocks of proteins, while phosphorus is critically involved in energy transfer processes, particularly through its role in ATP synthesis [3].

Sulfur is an essential macronutrient pivotal in various physiological processes critical for plant growth and development. It aids in seed production, chlorophyll formation, the development of root nodules in legumes, and the stabilization of protein structures. Additionally, sulfur is instrumental in the activation of numerous enzymes and contributes to the plant's ability to combat environmental stressors [4,5]. Sulfur deficiency can lead to significant disruptions in plant development, manifesting as stem shortening and thinning, inadequate branching, chlorosis in young leaves, reduced leaf size and quantity, stunted height, premature leaf drop, and a decrease in overall biomass [6]. Moreover, sulfur is a crucial component of several essential biomolecules within plants. It is found in amino acids such as L-cysteine and L-methionine, as well as in key coenzymes including S-adenosylmethionine, coenzyme A, biotin, and thiamine pyrophosphate. Sulfur also forms integral parts of prosthetic groups, such as iron-sulfur (Fe-S) centers, which are vital for the functionality of various enzymes involved in electron transfer and redox reactions. Furthermore, sulfur is fundamental in the biosynthesis of critical compounds such as glutathione, glucosinolates, and sulfolipids, which play roles in antioxidant defense, plant signaling, and defense against pathogens [7–9].

Given the critical role of sulfur as an essential element for plant development and the absence of enzymes responsible for its assimilation in animals, it has been proposed that enzymes involved in the sulfur metabolism, such as cysteine synthase (CS), cystathionine γ-synthase (CGS), and cystathionine β-lyase (CBL), represent promising targets for the development of novel herbicides [10]. These enzymes are crucial to the synthesis of sulfur-containing amino acids, which are vital for protein formation and other metabolic processes in plants. Targeting these enzymes offers a strategic avenue for herbicide development, as their absence in animals enables selective action against unwanted plant species while minimizing potential risks to animal health.

The development of new herbicide targets is of paramount importance, particularly given the increasing incidence of herbicide-resistant weed species. A significant number of species have shown resistance to commercial herbicides, with reports indicating that up to 21 different sites of action are ineffective against certain resistant populations [11,12]. Furthermore, the intensive and recurrent use of herbicides has selected weed biotypes resistant to multiple sites of action, greatly complicating effective weed management strategies [13]. While alternatives to traditional chemical herbicides exist, such as crop rotation, cover cropping, precision agriculture technologies (including nanotechnology), RNA interference, genetic engineering, and the use of bioherbicides [14,15], the development of a novel herbicide with a unique mechanism of action remains critically important. Such innovations

are essential for ensuring effective control of invasive weeds and safeguarding agricultural productivity, thus contributing to sustainable farming practices and food security.

In examining the sulfur assimilation pathway, there are additional enzymes, beyond those proposed by Hirase and Molin, involved in the conversion of sulfate to L-cysteine that could serve as promising targets for the development of herbicides with novel modes of action. The assimilation of sulfur occurs through several stages: the first step involves the activation of sulfate (SO_4^{2-}) by ATP sulfurylase (ATPS) to produce adenosine-5′-phosphosulfate (APS). Subsequently, APS can either be reduced to sulfite (SO_3^{2-}) by APS reductase or phosphorylated to 3′-phosphoadenosine-5′-phosphosulfate (PAPS) by APS kinase. Sulfite (SO_3^{2-}), a toxic intermediate, is rapidly reduced to sulfide (S^{2-}) by sulfite reductase (SiR) and incorporated into O-acetylserine (OAS) by O-acetylserine(thiol) lyase (OAS-TL) to produce L-cysteine cysteine [16–20]. Targeting these specific enzymes within the sulfur assimilation pathway holds great potential for developing novel herbicides that can selectively disrupt the growth of target weeds while minimizing the impact on non-target organisms.

Recently, our research group identified seven OAS-TL inhibitors through molecular docking and virtual screening strategies [21]. Among them, S-benzyl-L-cysteine (SBC) was characterized as a non-competitive inhibitor of Arabidopsis thaliana OAS-TL (AtOAS-TL), exhibiting inhibition constants of K_{ic} = 4.29 mM and K_{iu} = 5.12 mM. SBC markedly reduced cysteine biosynthesis both in vitro and in vivo in maize and *Ipomoea grandifolia*, ultimately suppressing plant growth [22]. Structurally, SBC contains a benzyl substituent bound to the sulfur atom of cysteine (–S–CH_2Ph), forming a thioether linkage that increases hydrophobicity and facilitates interaction with residues surrounding the sulfhydryl-binding region of the OAS-TL active site. In the present study, we investigated a structurally related analog, *O*-benzyl-serine (OBS), in which the benzyl group is attached to the oxygen atom of serine (–O–CH_2Ph), replacing sulfur with oxygen. This modification results in a more polar molecule capable of interacting with the OAS-binding pocket rather than the sulfide-binding site of OAS-TL. Molecular docking and dynamics simulations indicated that OBS can occupy the same binding region as the natural substrate OAS, forming hydrogen bonds with the catalytic Lys46–PLP complex, thus competing with OAS and disrupting cysteine biosynthesis through a substrate-competitive-like mechanism. Therefore, while both compounds share a benzylated amino acid backbone, their distinct heteroatom linkages (S vs. O) lead to different physicochemical properties and modes of inhibition. The selection of OBS as the research focus was driven by the hypothesis that replacing sulfur with oxygen could alter polarity, molecular recognition, and transport across cellular membranes, potentially yielding a molecule with herbicidal potential but a distinct mechanistic profile from SBC.

Building upon these mechanistic insights, the herbicidal potential of OBS was evaluated in two weed species, *Ipomoea grandifolia* and *Euphorbia heterophylla*, both of which perform C3 photosynthesis but differ markedly in morphology, growth dynamics, and metabolic plasticity. Preliminary enzymatic data revealed that *E. heterophylla* exhibits approximately 30-fold higher OAS-TL activity in roots and 6–7-fold higher activity in leaves compared to *I. grandifolia*. This intrinsic enzymatic disparity supports the hypothesis that OBS, as an OAS-TL inhibitor, would exert stronger inhibitory effects in *I. grandifolia*, which possesses lower basal OAS-TL activity and, therefore, reduced metabolic buffering capacity against enzyme inhibition. To test this hypothesis, we analyzed the differential physiological and biochemical responses of both species to OBS exposure using a set of quantifiable and integrative indicators, including (i) morphological and growth parameters (root and shoot length, fresh and dry biomass) to assess developmental sensitivity; (ii) OAS-TL activity and related enzymes of the sulfur assimilation pathway to verify biochemical inhibition; (iii) photosynthetic efficiency parameters obtained from light-response curves and chloro-

phyll a fluorescence to detect potential impairments in photochemical performance; and (iv) macro- and micronutrient accumulation patterns derived from ionomic profiling to identify systemic metabolic disturbances. Together, these complementary datasets were designed to establish a coherent framework linking OAS-TL inhibition to whole-plant physiological outcomes and to elucidate the species-specific determinants underlying differential sensitivity to OBS.

2. Materials and Methods

2.1. Molecular Dynamics Simulations

For the molecular dynamics (MD) simulations, we employed the three-dimensional structure of the maize OAS-TL enzyme, modeled as a homodimer complexed with the cofactor PLP and the substrate OAS, as previously described in [21]. The ligand OBS, whose poses had been selected in a prior molecular docking step, was manually positioned into the two catalytic sites of the enzyme, replacing the native substrate and generating the OAS-TL–OBS homodimeric complex.

In this stage, the molecular docking protocols were validated through the redocking of the native substrate OAS using AutoDock 4 and AutoDock Vina. Standard sampling and scoring algorithms were used in both programs, employing search boxes of 30 and 10 units and grid spacings of 0.375 Å and 1.0 Å, respectively. Redocking was repeated three times in each program, resulting in RMSD values of 0.95 ± 0.17 Å (AutoDock 4) and 0.31 ± 0.00 Å (AutoDock Vina), with corresponding docking scores of -6.93 ± 0.15 kcal/mol and -6.50 ± 0.00 kcal/mol. The same workflow was then applied to the inhibitor candidate OBS, yielding scores of -7.09 ± 0.12 kcal/mol (AutoDock 4) and -7.20 ± 0.00 kcal/mol (AutoDock Vina). OBS poses were reproducible across both tools, with RMSD values below 1.24 ± 0.48 Å. Based on its superior reproducibility, the pose obtained with AutoDock Vina was used as the starting conformation for the MD simulations.

This model was then submitted to the CHARMM-GUI server [23] to prepare all necessary simulation input files. A covalent bond between Lys46 and PLP was introduced, following the configuration observed in the *Arabidopsis thaliana* OAS-TL structure (PDB ID: 1Y7L) [24], resulting in the modified residue IT1P. The protein–ligand complex was subsequently solvated with TIP3P water in a rectangular box extending 15 Å beyond the outermost protein atoms, and the system was neutralized with counterions to achieve a final NaCl concentration of 0.15 mol L^{-1}.

MD simulations were performed using NAMD 3.0 [25]. The CHARMM36m force field was applied to the protein and the modified IT1P residue, while force-field parameters for the ligands were generated using SwissParam [26], considering protonation states at pH 7.0. Partial charges were calculated in aqueous phase with the ORCA package [27], using the B3LYP hybrid functional, the 6-311G basis set, and the TightSCF criterion to ensure convergence and improve accuracy.

System preparation consisted of five sequential stages. First, ligand and cofactor atoms remained fixed while 30,000 steps of conjugate-gradient minimization were applied to the remaining atoms. In the second stage, all constraints were removed, followed by an additional 10,000 minimization steps. The third stage consisted of solvent equilibration for 60 ps, and the fourth stage involved a further 30,000 steps of unconstrained minimization. The final configuration from this step served as the initial structure for the production simulations.

Equilibration was conducted under NPT conditions (1 atm, 300 K) for 100 ns on the Lovelace supercomputer at the National High-Performance Computing Center (CENAPAD), Campinas, Brazil. Trajectories were analyzed in terms of root-mean-square deviation (RMSD), radius of gyration (Rg), root-mean-square fluctuation (RMSF), and the frequency

of contacts between amino-acid residues and the ligand within a 4 Å cut-off. RMSF values were computed using the last 5 ns of the trajectories, corresponding to the equilibrated portion of the simulations.

2.2. Plant Cultivation and Determination of Biometric Parameters

The seeds were selected according to size and shape and underwent specific dormancy-breaking procedures for each species. Seeds of *I. grandifolia* were subjected to acid scarification by immersing them in 98% sulfuric acid for 40 min to break physical dormancy, followed by thorough rinsing with deionized water. Seeds of *E. heterophylla*, which do not require dormancy-breaking treatment, were simply washed thoroughly in water. The seeds were then evenly distributed on moistened germination paper with deionized water. Another layer of paper was placed over the seeds, rolled up, and placed in appropriate tubes to maintain moisture. The tubes were then placed in germination chambers at 30 °C for 48 h for *I. grandifolia*, and 25 °C for 72 h for *E. heterophylla*.

Viable seedlings obtained after germination were selected, measured, and transferred to adjustable supports designed for hydroponic cultivation. Each plant was maintained in 150 mL of a complete Hoagland and Arnon nutrient solution composed of the following macronutrient concentrations [28]: 1 mM KH_2PO_4, 5 mM KNO_3, 5 mM $Ca(NO_3)_2$, and 2 mM $MgSO_4$, supplying nitrogen (N), phosphorus (P), potassium (K), calcium (Ca), magnesium (Mg), and sulfur (S) in balanced proportions. The micronutrient supplement contained 0.5 mg L^{-1} boron (B), 0.5 mg L^{-1} manganese (Mn), 0.05 mg L^{-1} zinc (Zn), 0.02 mg L^{-1} copper (Cu), and 0.05 mg L^{-1} molybdenum (Mo), and iron was supplied as 0.1 mM Fe–EDTA to ensure adequate availability and stability. Plants were exposed to increasing OBS concentrations (0–500 µM), and the nutrient solution was renewed every 48 h to maintain chemical stability and consistent nutrient availability throughout the exposure period. After 12 days of cultivation, root length, stem length, leaf area, and the fresh and dry biomass of roots and shoots were recorded. Dry weight was obtained after dehydration of plant tissues at 70 °C until reaching constant mass.

2.3. Enzyme Activities of Sulfur Assimilation Pathway

Roots or leaves (0.1 g) were pulverized in liquid nitrogen and then homogenized with a buffer containing 50 mM Hepes/KOH pH 7.5; 10 mM KCl; 10 mM EDTA, 1 mM EGTA, 10% glycerin, 10 mM DTT, and 0.5 mM PMSF [29]. The homogenate was centrifuged at 15,000× *g* for 20 min, and the supernatant was used as an enzyme source.

The activity of OAS-TL was determined according to Randewig et al. [29]. Enzymatic extracts were first quantified for total protein content using the Bradford method, employing bovine serum albumin (BSA) as the standard. For each assay, 0.1 mL of enzymatic supernatant was mixed with 0.1 mL of reaction buffer composed of 50 mM HEPES (pH 7.5), 10 mM *O*-acetylserine, 15 mM Na_2S, and 5 mM DTT. The reaction mixture was incubated at 25 °C for 15 min, after which the reaction was stopped by adding 50 µL of 20% (*w*/*v*) trichloroacetic acid (TCA). Samples were then centrifuged at 10,000× *g* for 5 min, and 100 µL of the resulting supernatant was transferred to a new tube. To this aliquot, 100 µL of glacial acetic acid and 200 µL of freshly prepared ninhydrin reagent (250 mg ninhydrin dissolved in 6 mL concentrated acetic acid and 4 mL concentrated HCl) were added. The mixture was incubated in a boiling water bath for 10 min, followed by rapid cooling on ice. The absorbance was measured at 560 nm, and cysteine formation was quantified using a standard curve prepared with known concentrations of L-cysteine. Enzyme activities were expressed as specific activity (µmol × min^{-1} × mg $protein^{-1}$).

2.4. Gas Exchange and Chlorophyll a Fluorescence Analysis

Gas exchange measurements were carried out on the 12th day of cultivation using the first fully expanded leaf, defined as the first mature leaf located immediately below the youngest developing leaf, showing no measurable increase in leaf area over a 48 h period and exhibiting a fully unfolded lamina without residual juvenile curvature. Only leaves that met all these criteria were used for photosynthetic assessments. To assess the parameters, gas exchange, and multiphase fluorescence measurements were combined using a portable photosynthesis system equipped with a fluorometer (Li-6800, Li-Cor Inc., Lincoln, NE, USA) with a leaf chamber with a 2 cm^2 measurement area. The temperature inside the chamber was maintained at 25 °C, and the vapor pressure deficit between the air and leaf was controlled at 0.2 kPa, with a flow rate of 700 µmol s^{-1}. Measurements were conducted between 7:00 a.m. and 3:00 p.m., but only data collected during periods where the variables within the same experimental group remained stable were considered [22].

The gas exchange parameters measured included the CO_2 assimilation rate (A, µmol m^{-2} s^{-1}), transpiration (E, mmol m^{-2} s^{-1}), stomatal conductance (gs, mol m^{-2} s^{-1}), and intercellular CO_2 concentration (Ci, µmol mol^{-1}), which were derived from the light response curve (A/PPFD). The photosynthetically active photon flux density (PPFD) ranged from 2000 to 0 µmol photons m^{-2} s^{-1} with the following intensities: 2000, 1900, 1800, 1700, 1600, 1500, 1400, 1200, 1000, 800, 600, 400, 200, 175, 150, 125, 100, 75, 50, 25, and 0 µmol photons m^{-2} s^{-1}. Chamber conditions were adjusted to maintain a CO_2 concentration close to ambient levels (400 µmol mol^{-1}). From the A/PPFD curves, the following parameters were estimated: the quantum yield of photosynthesis [α, (µmol CO_2 m^{-2} s^{-1})/(µmol photons m^{-2} s^{-1})], maximum CO_2 assimilation rate (Amax), light compensation point (Pcomp), light saturation point (Psat), and respiration rate (Rd), using linear and hyperbolic mathematical models [30,31].

In parallel with gas exchange measurements, chlorophyll *a* fluorescence was also assessed [22]. After 25 to 30 min of light adaptation, the following parameters were measured: effective photochemical quantum efficiency (Fv′/Fm′), effective quantum yield (ϕPSII), electron transport rate in PSII (ETR), photochemical quenching (qP), and non-photochemical quenching (NPQ) [32]. These parameters were measured under an irradiance of 1400 µmol m^{-2} s^{-1} in two conditions of CO_2 concentration maintained in the leaf chamber (400 and 2000 µmol mol^{-1}). After 10 h of dark adaptation, initial fluorescence (Fo), maximum fluorescence (Fm), and maximum quantum yield of PSII (Fv/Fm) were determined, with Fv calculated as the difference between Fm and Fo [33]. The flash was set to a saturating red light of 8000 µmol m^{-2} s^{-1}, with three phases of 300 ms each and a ramp depth of 25%.

At each measurement point, data were recorded only after a stabilization period of 60–120 s, ensuring that all predefined stability criteria in the LI-6800 Log Setup were simultaneously satisfied. Stability was verified using three primary diagnostic parameters: ΔH_2O.Meas2 (slope limit = 0.5; standard deviation = 0.1; 20 s evaluation window), F.FlrLS (slope limit = 1.0; standard deviation = 1.0; 20 s window), and ΔCO_2.Meas2 (slope limit = 0.5; standard deviation = 0.1; 20 s window). Data logging proceeded only when all thresholds were met, confirming that the directly measured gas signals (CO_2 and H_2O) had reached true steady state. Because all derived physiological variables—such as photosynthetic rate, stomatal conductance, transpiration, and intercellular CO_2 concentration—are calculated from these primary measurements through embedded mathematical models, fulfilling these stability criteria ensures the accuracy, reproducibility, and biological reliability of both gas-exchange and fluorescence readings.

2.5. Determination of the Nutrient Content

To obtain the total contents of nutrients such as calcium (Ca), magnesium (Mg), iron (Fe), copper (Cu), zinc (Zn), manganese (Mn), phosphorus (P), potassium (K), and sulfur (S) in roots and leaves, digestion was performed using a nitric-perchloric solution. Sulfur was determined by the turbidimetric method with barium sulfate, according to Malavolta and colleagues [34]. The contents of Ca, Mg, Fe, Cu, Zn, Mn, P, and K were analyzed using microwave plasma atomic emission spectroscopy with the MP-AES 4200 (Agilent Technologies, Santa Clara, CA, USA).

2.6. Statistical Analysis

The data were expressed as the means of independent experiments ± standard error of the mean. The number of biological replicates varied according to the methodology: four to five independent plants per treatment were used for growth analyses; three biological replicates were used for ionomic measurements; seven plants per treatment were used for photosynthetic assessments; and five biological replicates were used for OAS-TL activity. Statistical analyses were performed using GraphPad Prism® v9 (GraphPad Software Inc., San Diego, CA, USA). Depending on the experimental design, data were analyzed using one-way ANOVA followed by Dunnett's multiple comparisons test or unpaired Student's *t*-test for pairwise comparisons. Differences were considered statistically significant at $p \leq 0.05$.

3. Results

3.1. Molecular Dynamics Simulations

Molecular dynamics simulations were performed to evaluate the stability of the modeled protein-ligand complexes and to analyze the contribution of individual residues in stabilizing the ligands bound to the enzyme's quaternary structure. The analysis focused on the homodimeric form of the enzyme in complex with either OAS or OBS. As illustrated in Figure 1a,b, both the protein backbone and the ligands remained stable throughout the final 40 ns of the simulation, exhibiting a root mean square deviation (RMSD) of approximately 3 Å. The radius of gyration of the protein backbone in both complexes remained stable, indicating that the ligands did not induce any unfolding of the protein (Figure 1c). Figure 1d presents the root mean square fluctuation (RMSF) for the alpha carbons of each residue, highlighting both the most flexible and stable regions of the protein. In the comparison between OAS and OBS, residues 208–218, which interact with OBS, displayed higher conformational fluctuations than when bound to OAS. Aside from this region and the terminal residues, there were no significant differences in RMSF values between the two complexes.

Further examination of the RMSF data helps clarify the biological relevance of the fluctuation observed for residues 208–218 in the OBS complex. Structural mapping of this segment shows that it corresponds to an extended and intrinsically flexible loop located away from the ligand-binding pocket. In contrast, the adjacent loop encompassing residues 219–240 directly contacts the ligand. Notably, this latter region exhibits reduced backbone fluctuation in the presence of OBS compared with OAS, indicating that OBS stabilizes the active site in a more closed conformation. This localized stabilization likely redistributes conformational dynamics toward the upstream 208–218 loop, accounting for its increased mobility. Overall, these data suggest that OBS binding imposes a distinct structural constraint on the catalytic-site architecture, potentially modulating substrate access and active-site breathing motions important for catalysis.

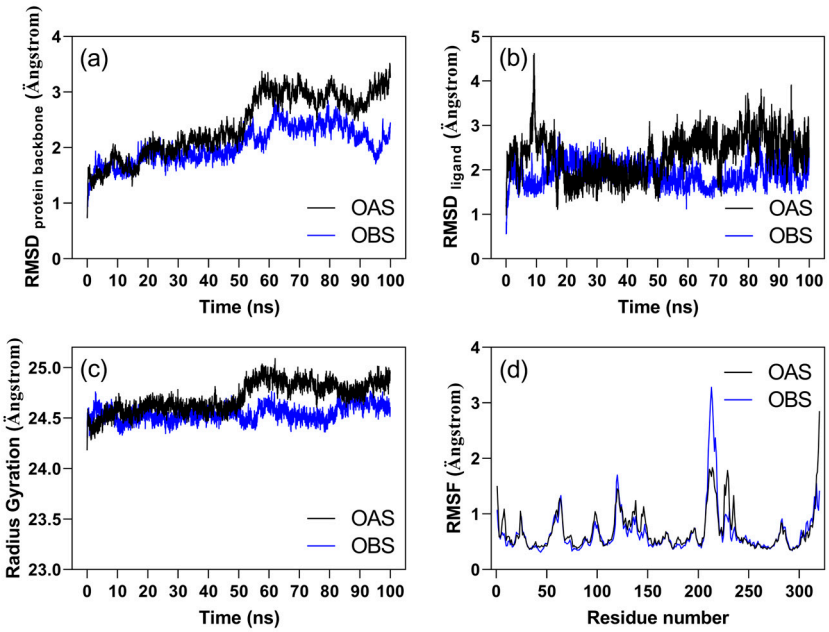


Figure 1. Trajectory analysis of molecular dynamics simulations for the OAS/ZmOAS-TL and OBS/ZmOAS-TL complexes over time, showing (**a**) RMSD of the protein backbone, (**b**) RMSD of the ligands, (**c**) radius of gyration of the protein backbone, and (**d**) RMSF of the alpha carbons of amino acid residues. The analyses represent the average values from both chains of the complexes.

Table 1 summarizes the contact frequency of ZmOAS-TL residues with the OAS and OBS ligands during the last 20 ns of the simulation, a phase in which the system achieved equilibrium (Figure 1). Notably, residues with more than 30% contact frequency with the ligands show distinct influences on each ligand. The residue IT1-46, corresponding to LYS-46 covalently linked to the cofactor PLP, demonstrated the highest contact frequency with both ligands (OAS and OBS). Additionally, THR-182 and GLY-181 also exhibited a high frequency of contact with both ligands. OAS showed significant interactions with residues GLY-225 and GLY-227, while OBS had higher contact frequencies with THR-74, GLY-76, ASN-77, THR-78, MET-125, PHE-148, GLY-181, and THR-182. Furthermore, variations in contact frequency between chains A and B suggest that interactions during the molecular dynamics simulations influence each chain reciprocally.

Table 1. Contact frequency of *Ipomoea grandifolia* OAS-TL residues with OAS and OBS ligands in the last 20 ns of molecular dynamics. Only contacts with a frequency greater than 5% are shown. The amino acid residues exhibiting the most frequent contacts in both chains are emphasized using bold formatting.

Residue	OAS Chain A	OAS Chain B	OBS Chain A	OBS Chain B
IT1-46	1.00	0.91	0.93	0.99
ILE-49	0.01	0.00	-	-
PRO-73	-	0.02	0.54	0.16
THR-74	0.01	0.10	0.68	0.70
SER-75	0.30	0.22	0.00	0.38
GLY-76	0.39	0.27	0.67	0.97
ASN-77	0.62	0.12	0.98	1.00
THR-78	0.89	0.26	0.99	0.98
MET-101	-	0.02	0.01	0.18

Table 1. *Cont.*

Residue	OAS Chain A	OAS Chain B	OBS Chain A	OBS Chain B
MET-125	0.01	0.02	0.69	0.72
GLN-147	0.18	0.10	0.92	0.11
PHE-148	0.39	0.06	0.77	0.54
GLY-181	0.58	0.66	0.78	0.33
THR-182	0.84	0.74	0.44	0.62
GLN-224	0.00	0.03	0.00	0.07
GLY-225	0.54	0.44	0.58	0.16
ILE-226	0.20	0.08	0.02	0.00
GLY-227	0.39	0.56	0.37	0.07
ALA-228	0.27	0.34	0.59	0.39
PHE-230	0.01	0.06	0.07	0.16

Analysis of the functional relevance of the residues identified in Table 1 help clarify the biological significance of the observed contact patterns. Residues Thr74, Ser75, Gln147, and the PLP-linked Lys46 (IT1-46) constitute key elements of the OAS-TL catalytic site [21]. Notably, OBS displayed high contact frequencies with Thr74 and the PLP cofactor, whereas OAS maintained strong interactions only with PLP. This shift in residue engagement indicates that OBS interacts more extensively with catalytic-site determinants, particularly within the substrate-binding region, suggesting that OBS may hinder the precise positioning of OAS required for catalysis. The distinct interaction profile of OBS therefore supports its potential to compromise enzymatic function through substrate-competitive displacement or active-site interference.

3.2. Effects of OBS on the Growth of Ipomoea grandifolia and Euphorbia heterophylla

The growth of *I. grandifolia* plants was significantly affected by treatment with OBS (Figure 2). Root length showed a dose-dependent reduction, ranging from 46% to 76% at concentrations of 62.5 to 500 µM (Figure 2a). Fresh and dry weights of the roots also decreased proportionally to the applied dose, with reductions of 53% to 88% in fresh weight (Figure 2b) and 29% to 76% in dry weight (Figure 2c) at concentrations of 62.5 to 500 µM of OBS.

The length of the aerial part did not show significant changes with OBS treatment (Figure 2d), but there was a reduction in fresh weight by 22% and 40% compared to the control at concentrations of 250 and 500 µM of OBS, respectively (Figure 2e). In contrast, the dry weight of the aerial part increased by 53% and 51% at concentrations of 125 and 250 µM of OBS, respectively (Figure 2f).

Leaf area could only be measured at 62.5 and 125 µM OBS, showing reductions of 52% and 93% compared to the control, respectively, as higher concentrations caused a marked inhibition of leaf expansion and pronounced morphological deformation, which precluded reliable measurements (Figure 2g). Leaf fresh weight decreased by 35%, 71%, and 92% at concentrations of 62.5, 125, and 250 µM of OBS, respectively (Figure 2h), while leaf dry weight declined by 17%, 73%, and 88% compared to the control at the same concentrations (Figure 2i).

OBS also affected the growth parameters of *E. heterophylla* (Figure 3). Root length was reduced by 19%, 47%, and 60% at concentrations of 62.5, 250, and 500 µM, respectively. Root fresh weight decreased by 32%, 60%, and 72% at concentrations of 125, 250, and 500 µM,

respectively, and root dry weight was reduced by 38% and 72% at concentrations of 250 and 500 µM, respectively.

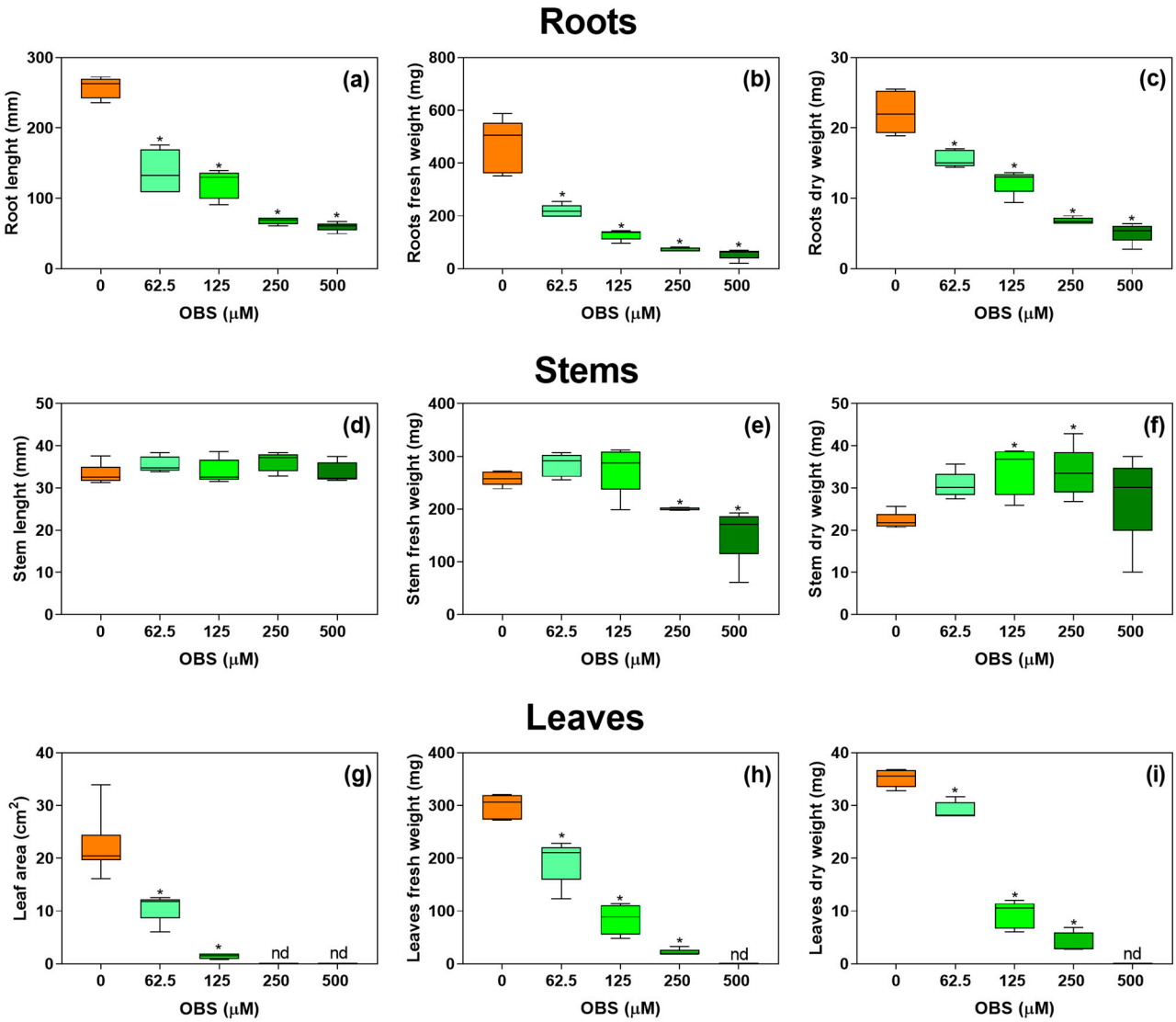


Figure 2. Effects of *O*-benzyl-L-serine (OBS) on the growth of *Ipomoea grandifolia* plants. Root length (**a**), root fresh weight (**b**), root dry weight (**c**), stem length (**d**), stem fresh weight (**e**), stem dry weight (**f**), leaf area (**g**), leaf fresh weight (**h**), and leaf dry weight (**i**) of *I. grandifolia* plants exposed to 0–500 µM OBS for 12 days. Data are presented as mean ± standard error of the mean (SEM) of 4 to 5 biological replicates. The asterisks indicate significant differences compared with the control ($p \leq 0.05$; Dunnett's multiple comparison test). Nd = not determined due to the small size of leaves.

In contrast, the length of the aerial part was stimulated compared to the control, with increases of 25%, 23%, and 23% at concentrations of 125, 250, and 500 µM, respectively. The fresh and dry weights of the aerial part were not significantly altered by OBS treatment. Importantly, the increase in stem length observed in *E. heterophylla* corresponded to a genuine elongation of the main stem. Morphological inspection of the treated plants confirmed that the measured axis was the primary stem, indicating that OBS stimulated axial elongation rather than artificially increasing total length through lateral shoot emergence.

Although the aerial part showed increased growth, leaf area was reduced in a dose-dependent manner, decreasing by 34% to 89% at concentrations of 62.5 to 500 µM compared to the control. Fresh and dry weights of leaves were reduced by OBS treatment starting at 125 µM, with reductions reaching 84% in fresh weight and 85% in dry weight.

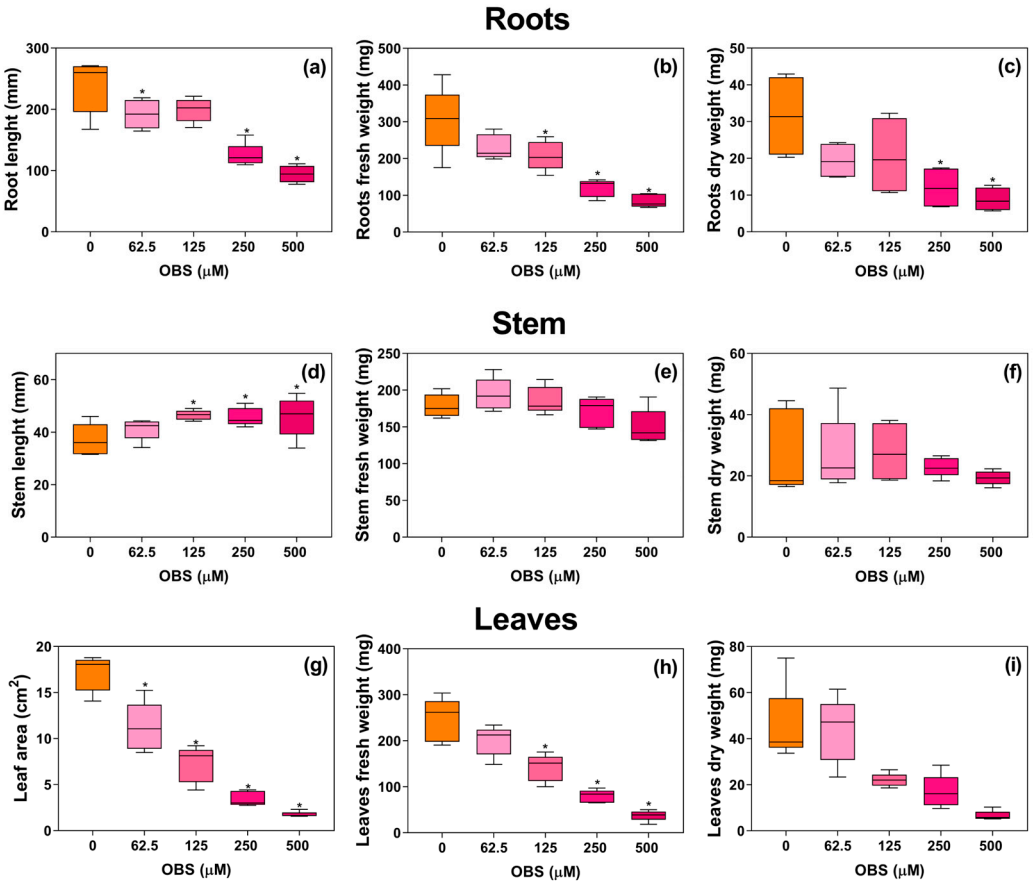


Figure 3. Effects of *O*-benzyl-L-serine (OBS) on the growth of *Euphorbia heterophylla* plants. Root length (**a**), root fresh weight (**b**), root dry weight (**c**), stem length (**d**), stem fresh weight (**e**), stem dry weight (**f**), leaf area (**g**), leaf fresh weight (**h**), and leaf dry weight (**i**) of *E. heterophylla* plants exposed to 0–500 μM OBS for 12 days. Data are presented as mean ± standard error of the mean (SEM) of 4 to 5 biological replicates. The asterisks indicate significant differences compared with the control ($p \leq 0.05$; Dunnett's multiple comparison test).

A thorough analysis of the morphology of plants treated with OBS revealed significant alterations in the development of *I. grandifolia* and *E. heterophylla* (Figures 4 and 5). The leaves of both species exhibited signs of chlorosis and curling, which were more pronounced at higher doses of OBS. There was also an increased number of shoots in plants treated with OBS. In *I. grandifolia*, shoots emerged from the development of axillary buds. In *E. heterophylla*, in addition to the increase in shoots from axillary buds, new shoots also emerged from lateral buds in various regions of the hypocotyl below the cotyledons.

3.3. Effects of the OBS on the Activities of OAS-TL of I. grandifolia and E. heterophylla Plants

The activity of OAS-TL in both roots and leaves of the studied species was modulated by OBS treatment (Figure 6). In *I. grandifolia*, OAS-TL activity in the roots decreased by 42% and 52% at concentrations of 125 μM and 250 μM, respectively (Figure 6a), while no significant changes were observed in the leaves. In contrast, in *E. heterophylla*, OAS-TL activity in the leaves was notably affected, showing a 75% increase at the 250 μM concentration (Figure 6d), with no effect on the roots.

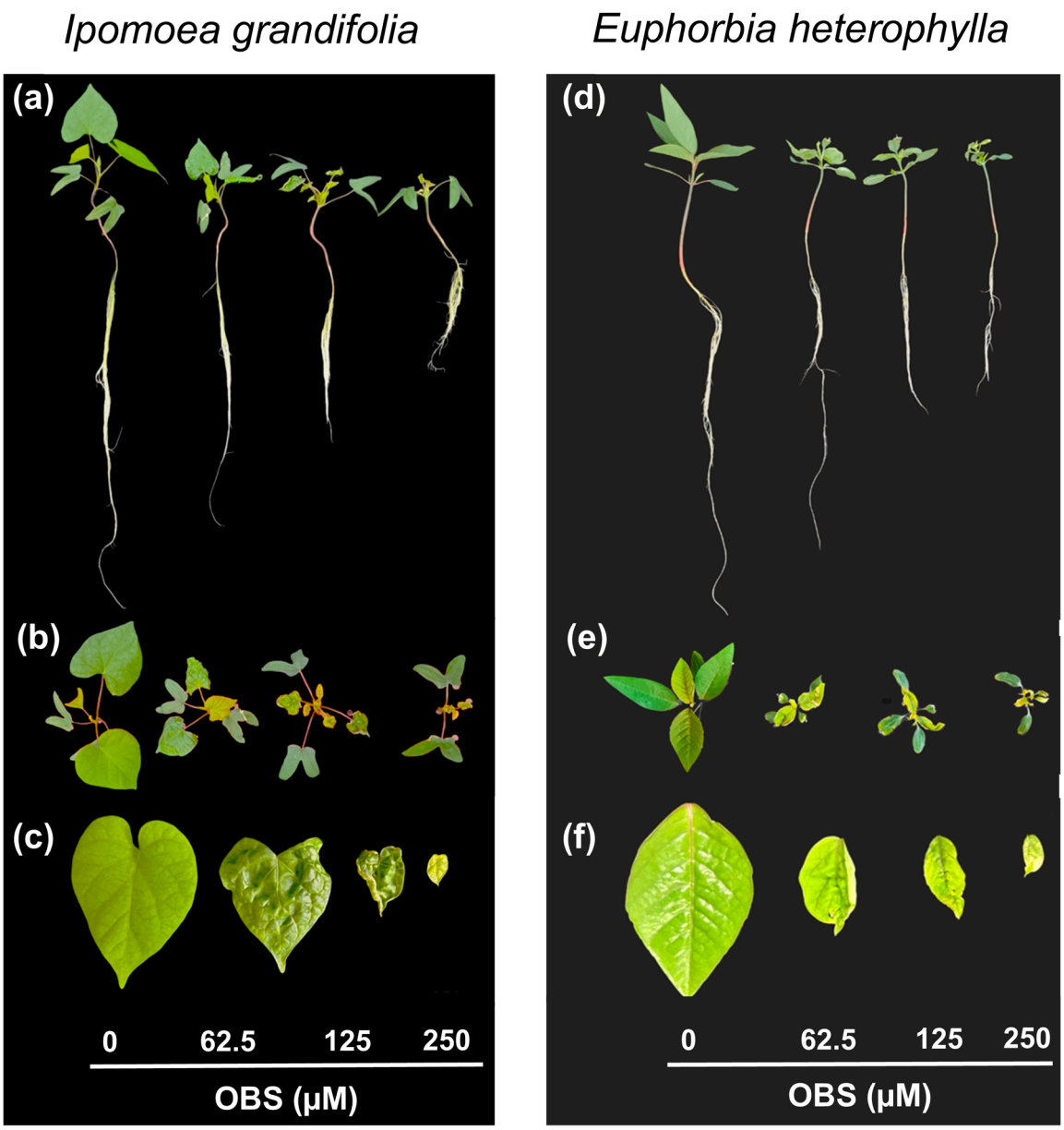


Figure 4. Representative images of *Ipomoea grandifolia* and *Euphorbia heterophylla* plants treated with increasing concentrations of *O*-benzyl-L-serine (OBS; 0, 62.5, 125, and 250 µM). Panels (**a**–**c**) correspond to *I. grandifolia* and panels (**d**–**f**) to *E. heterophylla*. Whole-plant views (**a**,**d**) show a progressive reduction in shoot length and overall vigor with increasing OBS concentration. Top-view images (**b**,**e**) reveal a marked decrease in leaf area and alterations in canopy architecture. Representative leaves (**c**,**f**) exhibit pronounced curling and deformation, indicating that OBS treatment induces visible morphological stress responses in both species.

3.4. Effects of OBS on Nutrient Content in the Roots and Leaves of I. grandifolia and E. heterophylla

OBS significantly altered the ionome of *I. grandifolia* and *E. heterophylla* plants (Figure 7). Several changes were observed in the roots of *I. grandifolia* (Figure 7a). Calcium (Ca) levels in the roots of *I. grandifolia* were reduced by 34% with the 62.5 µM OBS treatment, while magnesium (Mg) content decreased by 46% at the 125 µM concentration. Sulfur (S) levels dropped at both OBS concentrations, with 38% and 56% reductions at 62.5 and 125 µM, respectively. The effects differed when analyzing *I. grandifolia* leaves (Figure 7b). Magnesium (Mg) content decreased by 52% at 125 µM OBS, while iron (Fe) levels increased by 105% at the same concentration.

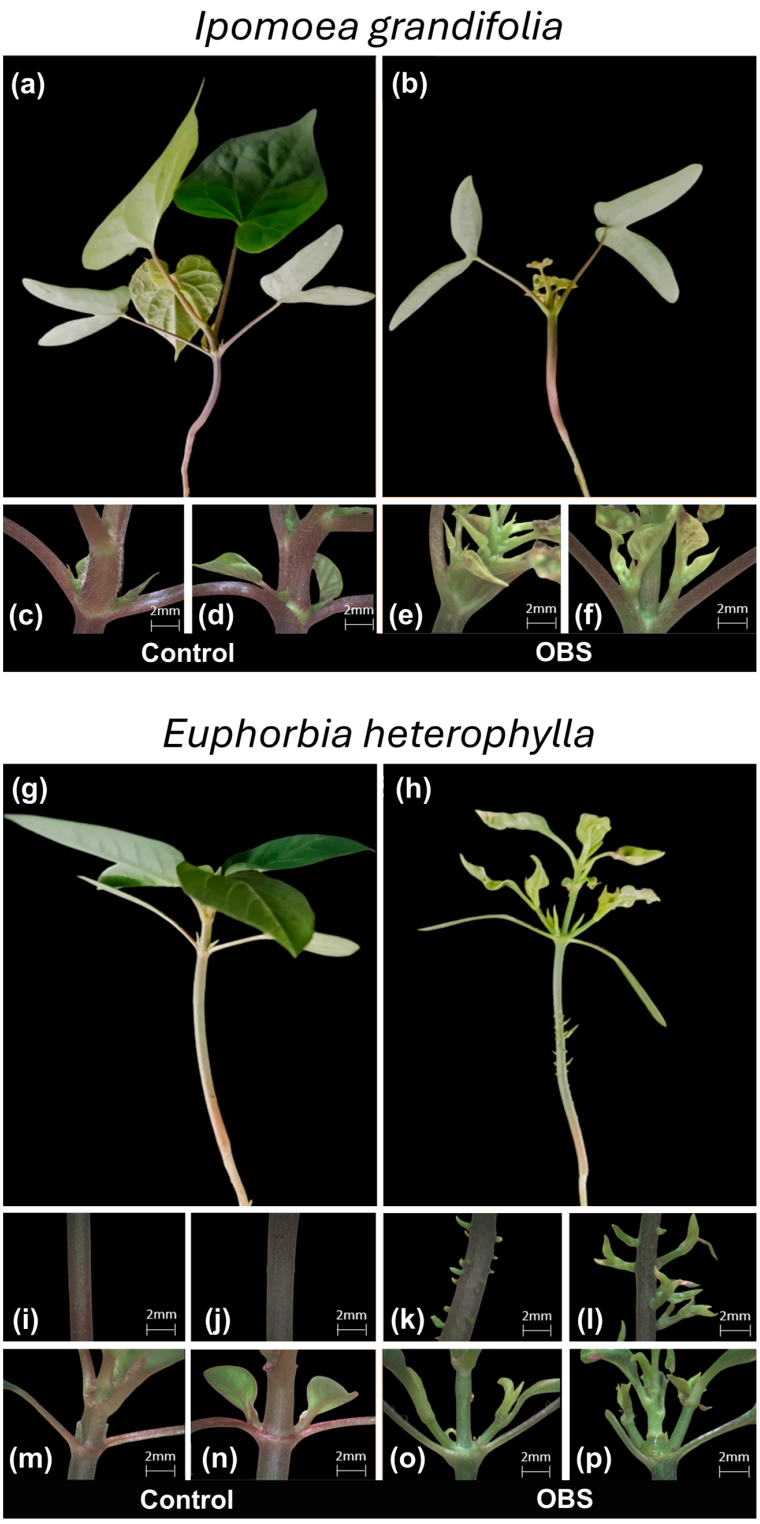


Figure 5. Representative photos of morphological changes observed in *Ipomoea grandifolia* (**a**–**f**) and *Euphorbia heterophylla* (**g**–**p**) plants treated with 62.5 µM *O*-benzyl-L-serine (OBS). Aerial part and first node (8× magnification) of untreated *I. grandifolia* plants (**a**,**c**,**d**); aerial part and first node (8× magnification) of plants treated with *O*-benzyl-L-serine (**b**,**e**,**f**). Aerial part and stem regions of untreated *E. heterophylla* plants (**g**,**i**,**j**,**m**,**n**); aerial part and stem regions of plants treated with *O*-benzyl-L-serine (**h**,**k**,**l**,**o**,**p**). Panels (**i**–**l**) highlight stem regions showing the emergence of lateral buds in OBS-treated plants, indicating loss of apical dominance. Panels (**c**–**f**) and (**m**–**p**) show 8× magnifications of the first node in *I. grandifolia* and *E. heterophylla*, respectively. OBS treatment caused pronounced leaf curling and morphological alterations compared with untreated controls.

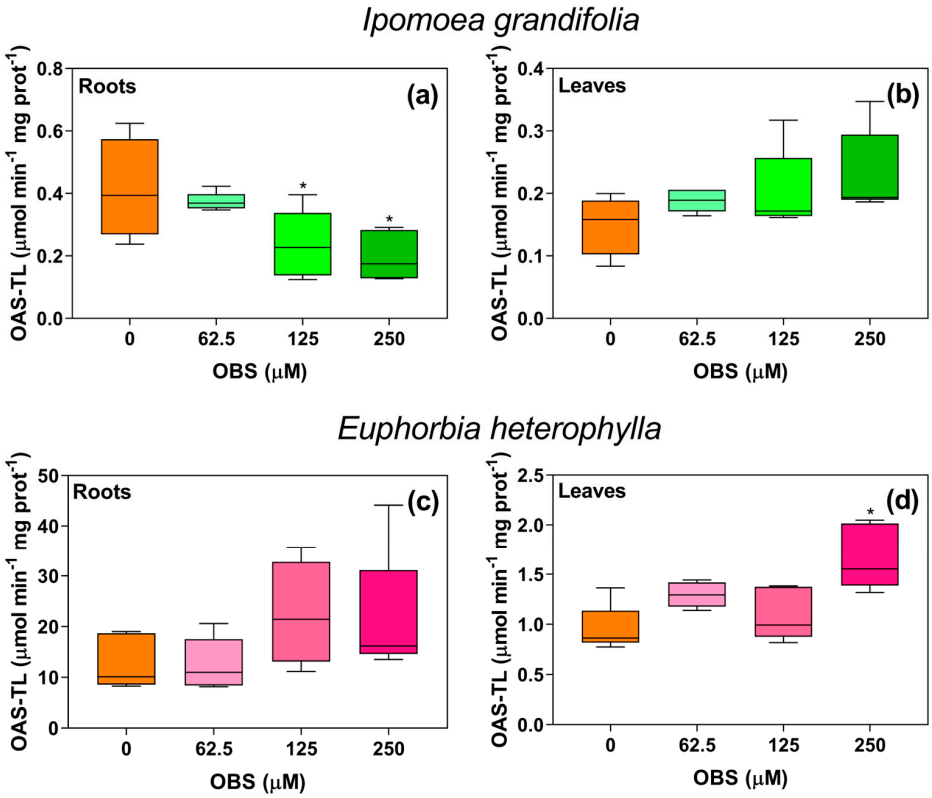


Figure 6. Effects of *O*-benzyl-L-serine (OBS) on *O*-acetylserine-(thiol)-lyase (OAS-TL) activity in *Ipomoea grandifolia* and *Euphorbia heterophylla* plants. Root OAS-TL activity of *I. grandifolia* (**a**), leaf OAS-TL activity of *I. grandifolia* (**b**), root OAS-TL activity of *E. heterophylla* (**c**), leaf OAS-TL activity of *E. heterophylla* (**d**). Plants were exposed to 62.5, 125, and 250 μM OBS for 12 days. Data are presented as mean ± standard error of the mean (SEM) of 5 biological replicates. The asterisks indicate significant differences compared with the control ($p \leq 0.05$; Dunnett's multiple comparison test).

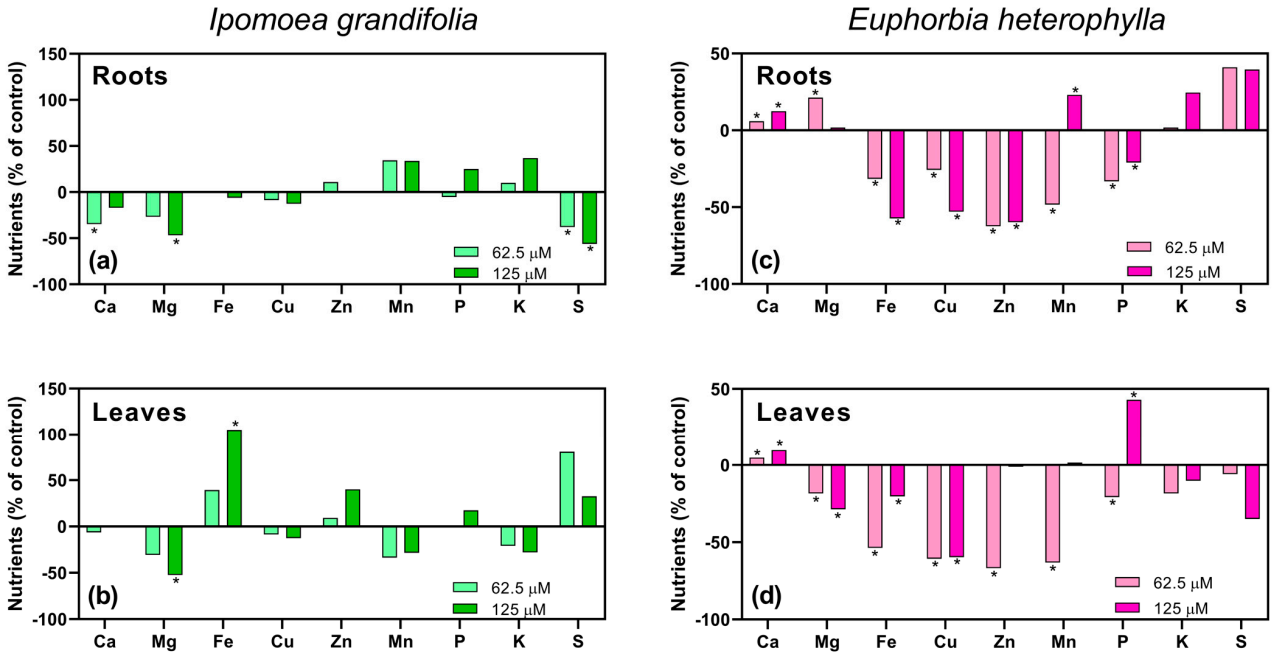


Figure 7. Effects of *O*-benzyl-L-serine (OBS) (62.5 or 125 μM) on nutrient levels in the roots and leaves of *Ipomoea grandifolia* and *Euphorbia heterophylla*. Nutrient levels in the roots of *I. grandifolia* (**a**), leaves of *I. grandifolia* (**b**), roots of *E. heterophylla* (**c**), and leaves of *E. heterophylla* (**d**). Data are presented as mean ± standard error of the mean (SEM) of 3 biological replicates. The asterisks indicate significant differences compared with the control ($p \leq 0.05$; Dunnett's multiple comparison test).

In *E. heterophylla*, alterations were also observed in both roots and leaves (Figure 7c,d). In the roots (Figure 7c), calcium (Ca) levels increased by 6% and 12% at 62.5 and 125 µM, respectively. Magnesium (Mg) content increased by 21% only at 62.5 µM. Iron (Fe) levels were reduced by 32% and 57% at 62.5 and 125 µM, respectively. Copper (Cu) levels decreased by 26% and 53%, while zinc (Zn) content dropped by 62% and 60%, at 62.5 µM and 125 µM, respectively. Manganese (Mn) levels were reduced by 48% at 62.5 µM but increased by 23% at 125 µM, while phosphorus (P) levels decreased by 33% and 20% at 62.5 µM and 125 µM, respectively.

In the leaves (Figure 7d), calcium (Ca) content increased by 5% and 10% at 62.5 and 125 µM, respectively. Magnesium (Mg) levels decreased by 18% and 29%, while iron (Fe) content was reduced by 54% and 20%, at 62.5 µM and 125 µM, respectively. Copper (Cu) levels dropped by 61% and 60% at 62.5 µM and 125 µM, respectively, while zinc (Zn) and manganese (Mn) levels were reduced only at 62.5 µM, by 67% and 63%, respectively. Phosphorus (P) content decreased by 21% at 62.5 µM but increased by 43% at 125 µM.

3.5. Effects of OBS on Photosynthetic Performance of I. grandifolia and E. heterophylla

The effects of OBS on the photosynthetic activity of *I. grandifolia* and *E. heterophylla* are shown in Figures 8–13. Figures 8 and 11 display the light response curves, along with the average values of stomatal conductance (gs), transpiration (E), and internal CO_2 concentration (Ci) (Figures 8b–d and 11b–d). When evaluating the light response curves, it is evident that in both species, the non-linear adjustment curve for control plants is very similar to that of the OBS-treated plants, with no significant change in CO_2 assimilation (A) as PPFD varied. In *I. grandifolia*, no alterations were observed in gs, E and Ci parameters. However, in *E. heterophylla*, OBS treatment reduced gs by 10% (Figure 11b) and E by 11% (Figure 11c).

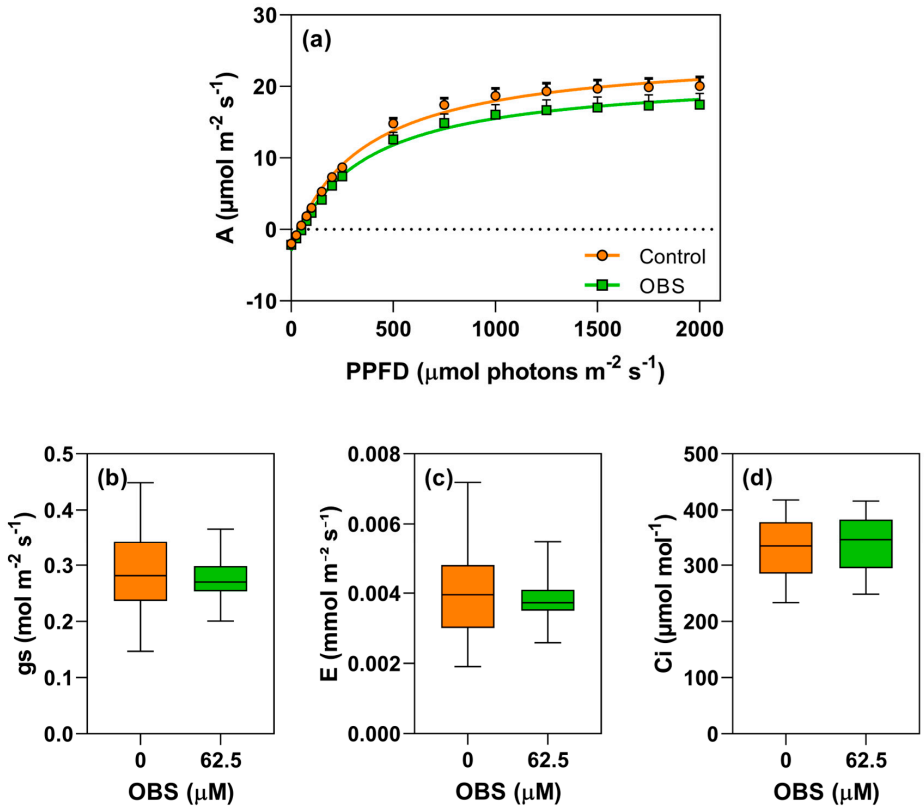


Figure 8. Effects of *O*-benzyl-L-serine (OBS) on *Ipomoea grandifolia* plants. CO_2 assimilation rate (A, µmol m^{-2} s^{-1}) in response to photosynthetically active photon flux density (PPFD) (**a**), stomatal

conductance (gs, mol m^{-2} s^{-1}) (**b**), transpiration rate (E, mmol m^{-2} s^{-1}) (**c**), and intercellular CO_2 concentration (Ci, µmol mol^{-1}) (**d**). Plants were exposed to 62.5 µM OBS for 12 days. Data are presented as mean ± standard error of the mean (SEM) of 7 biological replicates. $p \leq 0.05$; unpaired Student's *t*-test.

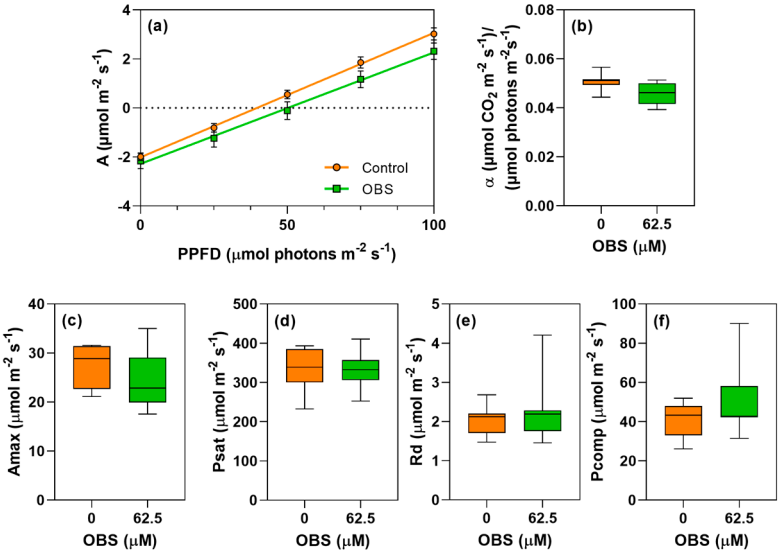


Figure 9. Effects of *O*-benzyl-L-serine (OBS) on *Ipomoea grandifolia* plants. Quantum productivity [(µmol CO_2 m^{-2} s^{-1})/(µmol photons m^{-2} s^{-1})] (**a**), quantum yield of photosynthesis (α) (**b**), maximum carbon assimilation rate (Amax, µmol CO_2 m^{-2} s^{-1}) (**c**), light saturation point (Psat, µmol m^{-2} s^{-1}) (**d**), respiration rate (Rd, µmol m^{-2} s^{-1}) (**e**), and light compensation point (Pcomp, µmol m^{-2} s^{-1}) (**f**). Plants were exposed to 62.5 µM OBS for 12 days. Data are presented as mean ± standard error of the mean (SEM) of 7 biological replicates. $p \leq 0.05$; unpaired Student's *t*-test.

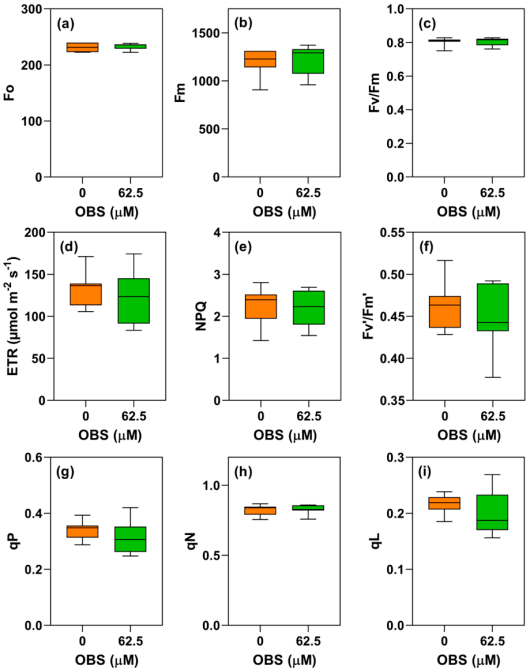


Figure 10. Effects of *O*-benzyl-L-serine (OBS) on *Ipomoea grandifolia* plants. Initial fluorescence (Fo) (**a**), maximum fluorescence (Fm) (**b**), maximum quantum yield of PSII (Fv/Fm) (**c**), electron transport rate (ETR) (**d**), non-photochemical quenching (NPQ) (**e**), effective photochemical quantum efficiency (Fv′/Fm′) (**f**), photochemical quenching (qP) (**g**), non-photochemical quenching (qN) (**h**), and fraction of open PSII reaction centers (qL) (**i**). Plants were exposed to 62.5 µM OBS for 12 days. Data are presented as mean ± standard error of the mean (SEM) of 7 biological replicates. $p \leq 0.05$; unpaired Student's *t*-test.

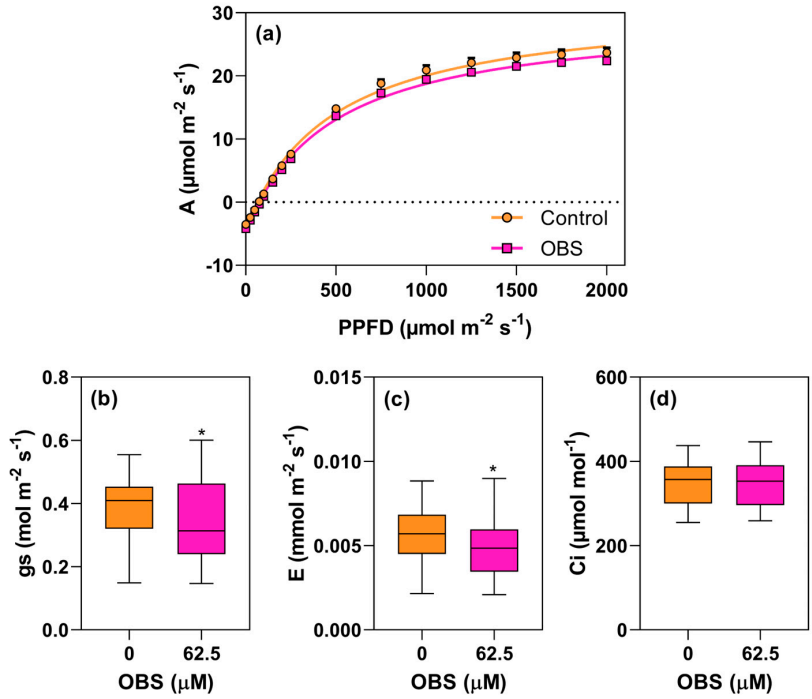


Figure 11. Effects of *O*-benzyl-L-serine (OBS) on *Euphorbia heterophylla* plants. CO_2 assimilation rate (A, µmol m^{-2} s^{-1}) in response to photosynthetically active photon flux density (PPFD) (**a**), stomatal conductance (gs, mol m^{-2} s^{-1}) (**b**), transpiration rate (E, mmol m^{-2} s^{-1}) (**c**), and intercellular CO_2 concentration (Ci, µmol mol^{-1}) (**d**). Plants were exposed to 62.5 µM OBS for 12 days. Data are presented as mean ± standard error of the mean (SEM) of 7 biological replicates. $* p \leq 0.05$; unpaired Student's *t*-test.

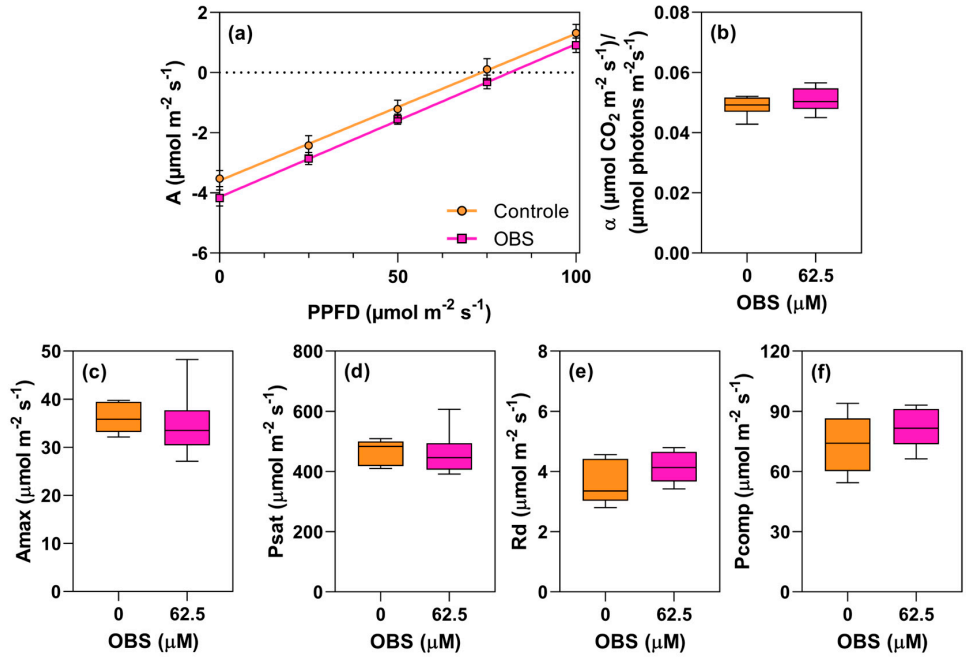


Figure 12. Effects of *O*-benzyl-L-serine (OBS) on *Euphorbia heterophylla* plants. Quantum productivity [(µmol CO_2 m^{-2} s^{-1})/(µmol photons m^{-2} s^{-1})] (**a**), quantum yield of photosynthesis (α) (**b**), maximum carbon assimilation rate (Amax, µmol CO_2 m^{-2} s^{-1}) (**c**), light saturation point (Psat, µmol m^{-2} s^{-1}) (**d**), respiration rate (Rd, µmol m^{-2} s^{-1}) (**e**), and light compensation point (Pcomp, µmol m^{-2} s^{-1}) (**f**). Plants were exposed to 62.5 µM OBS for 12 days. Data are presented as mean ± standard error of the mean (SEM) of 7 biological replicates. $p \leq 0.05$; unpaired Student's *t*-test.

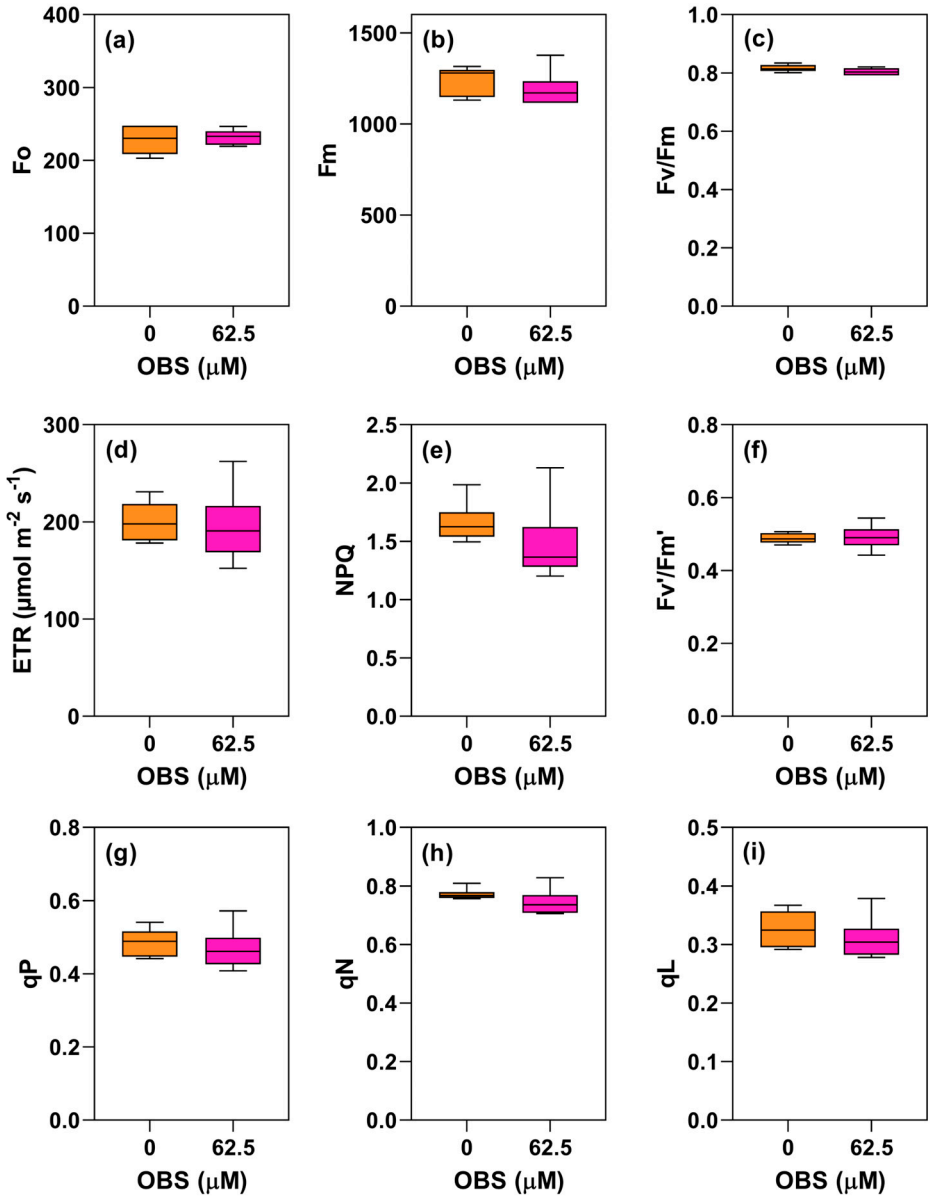


Figure 13. Effects of *O*-benzyl-L-serine (OBS) on *Euphorbia heterophylla* plants. Initial fluorescence (Fo) (**a**), maximum fluorescence (Fm) (**b**), maximum quantum yield of PSII (Fv/Fm) (**c**), electron transport rate (ETR) (**d**), non-photochemical quenching (NPQ) (**e**), effective photochemical quantum efficiency (Fv′/Fm′) (**f**), photochemical quenching (qP) (**g**), non-photochemical quenching (qN) (**h**), and fraction of open PSII reaction centers (qL) (**i**). Plants were exposed to 62.5 µM OBS for 12 days. Data are presented as mean ± standard error of the mean (SEM) of 7 biological replicates. $p \leq 0.05$; unpaired Student's *t*-test.

Figures 9 and 12 show the linear adjustment derived from the light response curves and related parameters, including α, Amax, Psat, Rd, and Pcomp. In both species, OBS treatment did not significantly alter any of these parameters.

Regarding chlorophyll *a* fluorescence, the data are presented in Figures 10 and 13, where Fo, Fm, Fv/Fm, ETR, NPQ, Fv'/Fm', qP, qN, and qL were measured. None of these parameters were affected by OBS treatment in either species.

4. Discussion

The present study demonstrated that OBS significantly affected the growth and metabolism of *I. grandifolia* and *E. heterophylla*, two weed species. OBS caused a dose-

dependent inhibition of root growth in both species, with more pronounced effects in *I. grandifolia*. The compound altered OAS-TL activity, particularly in *I. grandifolia* roots, where activity was significantly reduced, whereas *E. heterophylla* showed increased leaf OAS-TL activity at higher OBS concentrations. OBS also modified the ionome of both species, with changes in key macro- and micronutrients such as calcium, magnesium, and sulfur, which are consistent with the growth inhibition and morphological phenotypes observed. Despite these metabolic shifts, no significant effects were detected on photosynthetic parameters at the concentrations tested. Photosynthesis could only be measured at 62.5 µM OBS because at 125 µM leaf area was insufficient. Moreover, at 62.5 µM OBS, leaves did not exhibit sulfur deficiency symptoms. Collectively, these results support a functional model in which OBS primarily constrains plant performance through root growth inhibition, altered sulfur partitioning and nutrient homeostasis, and reduced leaf expansion, rather than through a direct impairment of leaf-level photosynthetic efficiency.

To assess the stability of OBS relative to the substrate OAS, molecular dynamics simulations were performed with OAS-TL prior to in vivo assays. Both ligands reached stability within 100 ns, and RMSD profiles indicated equilibrium of protein chains and ligands. Radius of gyration stabilization supported the integrity of the protein's quaternary structure, indicating no unfolding during ligand interactions. Ligands fluctuated within the active site without loss of binding. Some residues interacted more frequently with one ligand than the other, suggesting distinct binding features; thus, mutations at high-contact residues could affect inhibition efficiency. Overall, these simulations support stable occupancy of the catalytic pocket by OBS, consistent with its proposed capacity to modulate OAS-TL function, while not substituting for kinetic validation of inhibition.

When comparing growth responses of *I. grandifolia* (Convolvulaceae) and *E. heterophylla* (Euphorbiaceae) to OBS, *I. grandifolia* displayed higher sensitivity, indicating species-specific effects. Root inhibition reached ~70% in *I. grandifolia* versus ~60% in *E. heterophylla*. At the highest OBS concentration, inhibition in *I. grandifolia* prevented measurement of some leaf biometric parameters. In contrast, *E. heterophylla* exhibited a modest increase in stem length; morphological inspection confirmed true elongation of the primary stem rather than an artifact of lateral shoot emergence. These contrasting outcomes indicate differential physiological resilience to OBS-induced metabolic disturbance, consistent with prior evidence that herbicide specificity can arise from variation in metabolic pathways and sensitivity to sulfur-metabolism inhibitors [22,35].

A mechanistic basis for the higher sensitivity of *I. grandifolia* emerges from intrinsic enzymatic capacity. Preliminary assays showed that *E. heterophylla* has ~30-fold higher OAS-TL activity in roots and 6–7-fold higher activity in leaves than *I. grandifolia*. These differences imply distinct buffering capacity under OAS-TL interference. Higher constitutive OAS-TL activity may better sustain L-cysteine homeostasis under partial inhibition, via maintained cysteine production or compensatory flux through sulfur assimilation. Conversely, the lower basal OAS-TL activity in *I. grandifolia* narrows its metabolic margin, increasing vulnerability to reduced cysteine synthesis and associated growth suppression and nutrient imbalance. Thus, basal OAS-TL capacity provides a parsimonious biochemical explanation for stronger root inhibition and sulfur depletion in *I. grandifolia* under equivalent OBS exposure.

OBS was identified by docking and virtual screening as a potential OAS-TL inhibitor, targeting an enzyme that synthesizes L-cysteine, a precursor for sulfur-containing metabolites essential for redox balance and cellular homeostasis [36,37]. In our study, OBS reduced OAS-TL activity in *I. grandifolia* roots, indicating disruption of sulfur metabolism at the enzymatic level. This inhibition is consistent with the intrinsically low basal root OAS-TL activity in this species (~30-fold lower than in *E. heterophylla*), which likely reduces

buffering capacity and increases susceptibility to perturbations in cysteine biosynthesis. At present, it remains unclear whether reduced activity reflects direct OBS–enzyme interaction or indirect regulatory effects; gene expression profiling and in vitro kinetic analyses will be needed [35,37]. In contrast, leaf OAS-TL activity in *I. grandifolia* was not reduced, and a modest upward trend occurred across concentrations. Rather than indicating direct activation, this trend is consistent with an organ-level compensatory response to root sulfur limitation, supported by the observed decrease in root sulfur and accumulation in leaves, suggesting altered sulfur partitioning. Such adaptive responses under sulfur limitation are well documented [22,37]. Accordingly, we frame these organ-specific patterns as functional interpretations supported by ionomic and enzymatic data, while recognizing that molecular validation of OAS-dependent regulation will require dedicated transcript and metabolite analyses.

Recent studies with SBC, another putative OAS-TL inhibitor, showed strong photosynthetic impairment in *Z. mays* and *I. grandifolia*. In *Z. mays*, SBC induced sulfur deficiency phenotypes and decreased stomatal and non-stomatal parameters, including gs, E, Ci, Vcmax, Vpmax, J, and fluorescence metrics (Fo, Fm, Fv/Fm, ϕPSII, Fv′/Fm′, qP, ETR) [22]. SBC likely limited L-cysteine availability for Fe–S cluster synthesis in PSI/PSII/cytochrome b6f, impairing electron transport, and reduced expression of photosynthetic complexes and Calvin/C4 enzymes, decreasing CO_2 assimilation [21]. In contrast, OBS did not significantly alter photosynthetic parameters in either species at the tested concentrations. While SBC strongly reduced photosynthesis-related metrics, OBS showed a milder profile, with no significant changes in Fo, Fv/Fm, Fv′/Fm′, or ETR. These comparisons indicate that OBS, up to 62.5 µM, does not phenocopy SBC-driven damage to photosynthetic machinery and instead primarily affects growth and nutrient status, including marked root sulfur reduction in *I. grandifolia*.

OBS did not significantly alter OAS-TL activity in *I. grandifolia* leaves, and photosynthetic parameters remained unaffected. Photosynthesis was assessed only at 62.5 µM OBS, the highest dose allowing adequate leaf expansion. At this concentration, total leaf sulfur increased in *I. grandifolia*, whereas *E. heterophylla* showed only a slight reduction. Importantly, elevated total sulfur does not necessarily imply enhanced assimilation through OAS-TL. Rather, it may reflect compensatory sulfate uptake and translocation in response to reduced L-cysteine synthesis; if assimilation is constrained, sulfur may accumulate in inorganic/oxidized pools instead of thiols. Similar compensation has been reported under impaired sulfur metabolism and may explain increased total leaf sulfur despite root enzymatic inhibition. These results contrast with SBC, which limited photosynthesis by restricting assimilated sulfur required for Fe–S clusters in photosystems and Calvin-cycle enzymes [9,22,38]. Thus, total sulfur measurements should be interpreted as indicators of partitioning and accumulation, not necessarily of increased reduced-sulfur assimilation.

Interestingly, OBS did not alter root OAS-TL activity in *E. heterophylla* but increased leaf activity, accompanied by reduced root sulfur and increased leaf sulfur. The sulfur-metabolism responses of *I. grandifolia* and *E. heterophylla* therefore differed under OBS. In *I. grandifolia*, reduced root OAS-TL activity was associated with reduced root sulfur. In parallel, sulfur accumulation in leaves suggests redistribution toward aerial tissues. In *E. heterophylla*, increased leaf OAS-TL activity may represent an adaptive response supporting cysteine-related metabolism in leaves under sulfur stress. Because these patterns derive from enzyme activity and ionomics rather than direct gene/metabolite profiling, we interpret them as functional compensatory signatures rather than definitive regulatory mechanisms. Sulfur-containing compounds, notably L-cysteine, remain central to redox homeostasis and antioxidant capacity in both species.

Another key finding is that OBS did not alter leaf-level photosynthetic parameters in either species at 62.5 µM, the dose at which gas exchange could be reliably measured. The absence of changes in gas exchange and chlorophyll fluorescence contrasts with SBC-mediated impairment [22], suggesting that OBS does not directly damage core photosynthetic machinery under these conditions. Moderate chlorosis does not necessarily reduce photosynthetic efficiency per unit leaf area, since chlorophyll content often exceeds what is required for maximal CO_2 assimilation under non-saturating light. Thus, maintenance of A, gs, and ΦPSII at 62.5 µM is consistent with mild pigment loss. Instead, OBS primarily affected root growth, sulfur metabolism, and leaf expansion, implying that OAS-TL inhibitors may reduce plant performance via distinct routes depending on structure and mode of action [17,22]. Photosynthetic data could not be obtained at ≥125 µM because severe leaf miniaturization prevented sealing of the LI-6800 chamber, consistent with the dose-dependent reduction in leaf area up to 500 µM. This limitation reflects extreme morphological restriction rather than absence of physiological effects. Accordingly, OBS likely reduces whole-plant carbon gain predominantly by limiting photosynthetically active surface area, while preserving leaf-level efficiency in the remaining tissue [22,38]. We therefore avoid inferring enhanced Fe–S cluster maintenance from sulfur redistribution alone, which will require direct assessment of reduced-sulfur metabolites and Fe–S assembly status.

Importantly, OBS significantly altered the ionomic profile of roots and leaves in both species. *I. grandifolia* leaves showed curling, which correlated with decreased root calcium. Calcium deficiency increases membrane permeability and compromises meristematic growth, often causing leaf deformation and chlorosis [39]. Calcium also acts as an intracellular signal coordinating hormone-related developmental processes, including auxin-dependent growth [40]. Thus, calcium depletion provides a direct physiological link to the observed morphological defects, independent of assumptions about primary hormonal targets.

Magnesium deficiency in *I. grandifolia* leaves and roots likely contributed to chlorosis. At 125 µM OBS, magnesium reduction was significant; at 62.5 µM the decrease was not statistically significant, yet chlorosis was visible, possibly reflecting early pigment limitation or delayed electron transport [41]. Despite this, photosynthetic parameters at 62.5 µM were not significantly altered, indicating that magnesium depletion did not reach a threshold limiting photosynthesis. Higher doses such as 125 µM, where depletion was stronger, could potentially impair photosynthetic function [42]. This pattern supports a dose-dependent separation between visible chlorosis and measurable leaf-level photosynthetic decline under OBS exposure.

The ionomic profile of *E. heterophylla* was more affected than that of *I. grandifolia*. OBS reduced iron, copper, zinc, and manganese, essential micronutrients for development [43]. In *I. grandifolia*, leaf chlorosis cannot be attributed to Fe shortage, since total Fe increased by 105% at 125 µM. This paradox is consistent with functional iron deficiency due to impaired Fe utilization. Although total leaf sulfur was not reduced, likely OAS-TL interference can compromise L-cysteine and downstream metabolites including SAM, required for tetrapyrrole/chlorophyll biosynthesis. In parallel, OBS reduced leaf Mg, the central atom of chlorophyll. Together, Mg limitation and reduced-sulfur metabolic constraints provide a coherent explanation for chlorosis independent of Fe deprivation. Copper, zinc, and manganese deficiencies can impair growth and biomass accumulation [44–47]. In our study, marked reduction in these micronutrients in *E. heterophylla*, likely due to impaired absorption, contributed to poor leaf development under OBS.

Both species exhibited loss of apical dominance, with reduced primary growth and emergence of lateral shoots (Figures 4 and 6). This phenotype is consistent with altered auxin–cytokinin balance, which regulates branching [48,49]. Auxin from the apical meris-

tem inhibits axillary buds, while cytokinins promote branching [50,51]. The OBS phenotype resembles scenarios where auxin transport is reduced and cytokinin action becomes relatively dominant. However, rather than asserting a direct hormonal target, we interpret apical dominance loss as an outcome compatible with nutrient imbalance and sulfur metabolic stress, both of which are known to modulate auxin transport and cytokinin responsiveness [48–51].

Beyond shoot architecture, OBS reduced root and leaf development and biomass, indicating broad growth inhibition. In *I. grandifolia*, reduced root sulfur is consistent with constrained sulfur assimilation, limiting synthesis of sulfur-containing amino acids such as L-cysteine and L-methionine, thereby restricting protein synthesis and growth. In *E. heterophylla*, growth inhibition was less severe, consistent with higher basal OAS-TL activity. Leaf OAS-TL activity increased at 250 μM OBS while root activity remained unchanged, a pattern intriguing for an inhibitor. One plausible explanation is compensatory feedback aimed at restoring cysteine biosynthesis, potentially involving increased OAS-TL expression in leaves. Because this inference is not directly supported by transcript data, we treat it as a functional compensatory interpretation supported by enzyme activity and sulfur partitioning patterns, rather than as a confirmed transcriptional mechanism. Nonetheless, this response was insufficient to sustain normal growth, as shown by reduced biometric parameters.

In *E. heterophylla*, although biometric parameters were also reduced compared to control plants, the effects were less pronounced than those observed in *I. grandifolia*. A key difference between the two species lies in the activity of OAS-TL. In leaves of *E. heterophylla* treated with 250 μM OBS, OAS-TL activity increased, contrasting with the unchanged activity detected in the roots. This finding is intriguing, considering that OBS was initially identified as an OAS-TL inhibitor. One plausible explanation for this paradoxical increase in enzymatic activity is that OBS might trigger a compensatory feedback response aimed at restoring cysteine biosynthesis. In this scenario, the plant could upregulate OAS-TL gene expression in the leaves to counterbalance the inhibited sulfur assimilation occurring in other tissues, particularly the roots. Although speculative in the absence of transcriptomic evidence, such an adaptive upregulation would be consistent with the plant's attempt to preserve sulfur homeostasis under metabolic stress. Nevertheless, this compensatory mechanism appears insufficient to sustain normal growth, as reflected by the overall reduction in biometric parameters.

Thus, although OBS was identified as an OAS-TL inhibitor, its effects varied by organ and species. Contrasting responses underscore species-specific coping mechanisms to sulfur -metabolism disruption. In *E. heterophylla*, increased leaf OAS-TL activity may reflect adaptive feedback supporting cysteine -related metabolism under constraint. In the absence of gene expression evidence, we frame this as a hypothesis grounded in enzyme activity and ionomic redistribution, and we avoid asserting transcriptional upregulation as a conclusion. Ionomic analyses showed that OBS also altered macro- and micronutrients in roots and leaves; deficiencies in Mg and Ca may aggravate growth impairment given their roles in membrane stability, development, and photosynthetic competence.

Moreover, altered nutrient uptake and distribution, particularly Mg and Ca, can further affect signaling pathways. Calcium is a central secondary messenger, and reduced Ca can impair developmental and stress signaling, compounding growth defects. Magnesium limitation can contribute to chlorosis and potentially affect photosynthesis at higher stress levels. Other phytohormones (e.g., gibberellins and abscisic acid) might also contribute to growth inhibition under metabolic stress. Because these hormonal components were not measured, we discuss them as plausible downstream contributors rather than pri-

mary mechanistic claims, emphasizing that targeted hormone profiling will be required to validate this dimension of OBS action.

Although the present study provides important insights into the physiological and biochemical effects of OBS, several limitations must be acknowledged. Hydroponics was used to maximize exposure and avoid soil confounders, but it does not capture agricultural complexity; thus, environmental fate and performance in soil remain unknown. Effects on non-target organisms and selectivity were not assessed. From a molecular perspective, this study did not determine whether OAS-TL modulation results from direct ligand–enzyme interaction or regulatory control; therefore, gene expression profiling and in vitro kinetics using purified OAS-TL will be required. Organ-specific responses also remain partially unresolved, and future work should examine sulfur transport dynamics and OAS-dependent signaling under OBS. Importantly, the current dataset provides functional, integrative evidence (enzyme activity, ionomics, and physiology) supporting sulfur-metabolism interference by OBS, while explicitly delimiting mechanistic claims that require additional molecular validation. Collectively, these limitations reinforce the need for soil-based trials, fate studies, ecotoxicology, and multi-omics approaches to determine the agronomic potential and ecological safety of OBS as a prototype herbicidal scaffold targeting sulfur metabolism.

5. Conclusions

This study shows that OBS induces consistent biochemical and physiological signatures compatible with interference in sulfur metabolism in a species- and organ-dependent manner, supporting OAS-TL as a promising target for herbicide discovery. The distinct responses of *Ipomoea grandifolia* and *Euphorbia heterophylla* highlight the plasticity of sulfur assimilation and its coupling with nutrient homeostasis. Beyond growth inhibition, OBS induced imbalances in sulfur, magnesium, and calcium, associated with morphological changes such as loss of apical dominance and chlorosis, while leaf-level photosynthetic performance remained largely preserved at the highest sublethal dose measurable (62.5 μM). Rather than implying a simple depletion of L-cysteine or photosynthetic cofactors, the combined enzyme activity and ionomic data support a functional model in which OBS promotes compensatory shifts in sulfur partitioning and stress-related metabolic adjustment. However, the increased OAS-TL activity observed in *E. heterophylla* leaves and the maintenance of photosynthetic activity indicate that regulatory responses remain unresolved. Future work should combine in vitro enzyme kinetics with purified OAS-TL, gene expression analyses, and targeted metabolomics of sulfur-containing compounds to determine whether OBS acts through direct enzymatic inhibition or indirect signaling. Hormone profiling and nutrient transport assays will also be important to mechanistically link sulfur/nutrient imbalance to architectural outcomes. Overall, this work advances the understanding of sulfur -metabolism interference in weeds and identifies OBS as a valuable scaffold for designing selective herbicides targeting underexplored metabolic nodes. At the same time, the relatively high effective concentrations, the lack of soil-based validation, and the absence of selectivity/ecotoxicology data indicate that OBS should be regarded primarily as a prototype guiding the development of more potent, stable, and selective OAS-TL inhibitors rather than a final herbicidal product.

Author Contributions: Conceptualization, R.M., O.F.-F. and R.P.C.; methodology, I.d.C.C., A.P.F., A.P.B., A.P.d.S.M., C.M.C., M.A.S.d.O., L.F.T., M.A.B. and J.H.V.d.A.J.; validation, R.M., O.F.-F. and P.S.A.B.; formal analysis, I.d.C.C., A.P.F., A.P.B. and A.C.C.; investigation, I.d.C.C., A.P.B., A.P.d.S.M., C.M.C., C.B. and A.C.C.; resources, O.F.-F. and R.M.; data curation, I.d.C.C.; writing—original draft preparation, I.d.C.C. and R.M.; writing—review and editing, R.M., O.F.-F. and W.D.d.S.; visualization, I.d.C.C. and R.M.; supervision, R.M. and O.F.-F.; project administration, R.M. and O.F.-F.; funding acquisition, O.F.-F. and R.P.C. All authors have read and agreed to the published version of the manuscript.

Funding: This research was funded by the Coordination for the Improvement of Higher Education Personnel–Brazil (CAPES, Finance Code 001), National Council for Scientific and Technological Development (CNPq; Grant 402480/2025-2).

Institutional Review Board Statement: Not applicable.

Informed Consent Statement: Not applicable.

Data Availability Statement: The raw data supporting the conclusions of this article will be made available by the authors on request.

Acknowledgments: Rogério Marchiosi, Wanderley Dantas dos Santos and Osvaldo Ferrarese-Filho are researchers of the National Council for Scientific and Technological Development (CNPq). The authors thank Antonio Nunis da Silva for technical assistance.

Conflicts of Interest: The authors declare no conflicts of interest.

Abbreviations

The following abbreviations are used in this manuscript:

ABS/RC	Absorbed energy flux per active reaction center
ADH	Aldehyde dehydrogenase
ATP	Adenosine triphosphate
CAT	Catalase
Chl a	Chlorophyll *a*
Cys	L-Cysteine
DAO	Diamine oxidase
DI_0/RC	Dissipated energy flux per reaction center
ETR	Electron transport rate
ET_0/RC	Electron transport flux per reaction center
Fo	Minimal fluorescence yield of dark-adapted state
Fm	Maximal fluorescence yield of dark-adapted state
Fv/Fm	Maximum quantum efficiency of PSII photochemistry
GSH	Glutathione (reduced form)
HMT	Histamine N-methyltransferase
H_2O_2	Hydrogen peroxide
JIP	Fast chlorophyll a fluorescence transient (OJIP curve)
MD	Molecular dynamics
OBS	*O*-Benzyl-serine
OAS	*O*-Acetylserine
OAS-TL	*O*-Acetylserine(thiol)-lyase
OJIP	Chlorophyll *a* fluorescence induction curve (O–J–I–P phases)
PEPC	Phosphoenolpyruvate carboxylase
PSII	Photosystem II
RC	Reaction center
RE_0/RC	Electron flux reducing end acceptors at PSI per reaction center
ROS	Reactive oxygen species
RuBisCO	Ribulose-1,5-bisphosphate carboxylase/oxygenase

SOD	Superoxide dismutase
TR_0/RC	Trapped energy flux per reaction center

References

1. Grusak, M.A. Plant Macro- and Micronutrient Minerals. In *Encyclopedia of Life Sciences*; Wiley-Blackwell: Hoboken, NJ, USA, 2001; pp. 1–5. [CrossRef]
2. Rengel, Z.; Cakmak, I.; White, P.J. *Marschner's Mineral Nutrition of Plants*; Academic Press: Cambridge, MA, USA, 2022; ISBN 0323853528.
3. Samota, M.K.; Navnage, N.P.; Bhatt, L. Role of Macro and Micronutrient in Development and Growth of Plant. *Trends Biosci.* **2017**, *10*, 3171–3173.
4. Uchida, R. Essential Nutrients for Plant Growth: Nutrient Functions and Deficiency Symptoms. *Plant Nutr. Manag. Hawaii's Soils* **2000**, *4*, 31–55.
5. Narayan, O.P.; Kumar, P.; Yadav, B.; Dua, M.; Johri, A.K. Sulfur Nutrition and Its Role in Plant Growth and Development. *Plant Signal. Behav.* **2023**, *18*, 2030082. [CrossRef]
6. Shah, S.H.; Islam, S.; Mohammad, F. Sulphur as a Dynamic Mineral Element for Plants: A Review. *J. Soil Sci. Plant Nutr.* **2022**, *22*, 2118–2143. [CrossRef]
7. Kopriva, S.; Mugford, S.G.; Baraniecka, P.; Lee, B.; Matthewman, C.A.; Koprivova, A. Control of Sulfur Partitioning between Primary and Secondary Metabolism in Arabidopsis. *Front. Plant Sci.* **2012**, *3*, 30360. [CrossRef] [PubMed]
8. Kopriva, S.; Malagoli, M.; Takahashi, H. Sulfur Nutrition: Impacts on Plant Development, Metabolism, and Stress Responses. *J. Exp. Bot.* **2019**, *70*, 4069–4073. [CrossRef] [PubMed]
9. Koprivova, A.; Kopriva, S. Molecular Mechanisms of Regulation of Sulfate Assimilation: First Steps on a Long Road. *Front. Plant Sci.* **2014**, *5*, 589. [CrossRef] [PubMed]
10. Hirase, K.; Molin, W.T. Sulfur Assimilation in Plants and Weed Control: Potential Targets for Novel Herbicides and Action Sites of Certain Safeners. *Weed Biol. Manag.* **2003**, *3*, 147–157. [CrossRef]
11. Tafoya-Razo, J.A.; Oregel-Zamudio, E.; Velázquez-Márquez, S.; Torres-García, J.R. 10,000-Times Diluted Doses of ACCase-Inhibiting Herbicides Can Permanently Change the Metabolomic Fingerprint of Susceptible *Avena fatua* L. Plants. *Plants* **2019**, *8*, 368. [CrossRef]
12. Qu, R.Y.; He, B.; Yang, J.F.; Lin, H.Y.; Yang, W.C.; Wu, Q.Y.; Li, Q.X.; Yang, G.F. Where Are the New Herbicides? *Pest Manag. Sci.* **2021**, *77*, 2620–2625. [CrossRef]
13. Ofosu, R.; Agyemang, E.D.; Márton, A.; Pásztor, G.; Taller, J.; Kazinczi, G. Herbicide Resistance: Managing Weeds in a Changing World. *Agronomy* **2023**, *13*, 1595. [CrossRef]
14. Perotti, V.E.; Larran, A.S.; Palmieri, V.E.; Martinatto, A.K.; Permingeat, H.R. Herbicide Resistant Weeds: A Call to Integrate Conventional Agricultural Practices, Molecular Biology Knowledge and New Technologies. *Plant Sci.* **2020**, *290*, 110255. [CrossRef] [PubMed]
15. Westwood, J.H.; Charudattan, R.; Duke, S.O.; Fennimore, S.A.; Marrone, P.; Slaughter, D.C.; Swanton, C.; Zollinger, R. Weed Management in 2050: Perspectives on the Future of Weed Science. *Weed Sci.* **2018**, *66*, 275–285. [CrossRef]
16. Capaldi, F.R.; Gratão, P.L.; Reis, A.R.; Lima, L.W.; Azevedo, R.A. Sulfur Metabolism and Stress Defense Responses in Plants. *Trop. Plant Biol.* **2015**, *8*, 60–73. [CrossRef]
17. Gigolashvili, T.; Kopriva, S. Transporters in Plant Sulfur Metabolism. *Front. Plant Sci.* **2014**, *5*, 442. [CrossRef]
18. Hell, R.; Wirtz, M. Molecular Biology, Biochemistry and Cellular Physiology of Cysteine Metabolism in *Arabidopsis thaliana*. *Arab. B* **2011**, *9*, e0154. [CrossRef]
19. Jobe, T.O.; Zenzen, I.; Rahimzadeh Karvansara, P.; Kopriva, S. Integration of Sulfate Assimilation with Carbon and Nitrogen Metabolism in Transition from C3 to C4 Photosynthesis. *J. Exp. Bot.* **2019**, *70*, 4211–4221. [CrossRef]
20. Long, S.R.; Kahn, M.; Seefeldt, L.; Tsay, Y.-F.; Kopriva, S. Nitrogen and Sulfur. In *Biochemistry and Molecular Biology of Plants*; Buchanan, B., Gruissem, W., Jones, R., Eds.; John Wiley & Sons: Hoboken, NJ, USA, 2015; pp. 711–768, ISBN 9780470714218.
21. Foletto-Felipe, M.d.P.; Abrahão, J.; Siqueira-Soares, R.d.C.; Contesoto, I.d.C.; Grizza, L.H.E.; de Almeida, G.H.G.; Constantin, R.P.; Philippsen, G.S.; Seixas, F.A.V.; Bueno, P.S.A.; et al. Inhibition of *O*-Acetylserine (Thiol) Lyase as a Promising New Mechanism of Action for Herbicides. *Plant Physiol. Biochem.* **2023**, *204*, 108127. [CrossRef]
22. Foletto-Felipe, M.d.P.; Abrahão, J.; Contesoto, I.d.C.; Ferro, A.P.; Grizza, L.H.E.; Menezes, P.V.M.d.C.; Wagner, A.L.S.; Seixas, F.A.V.; de Oliveira, M.A.S.; Tomazini, L.F.; et al. Inhibition of Sulfur Assimilation by S-Benzyl-L-Cysteine: Impacts on Growth, Photosynthesis, and Leaf Proteome of Maize Plants. *Plant Physiol. Biochem.* **2024**, *216*, 109173. [CrossRef]
23. Jo, S.; Kim, T.; Iyer, V.G.; Im, W. CHARMM-GUI: A Web-based Graphical User Interface for CHARMM. *J. Comput. Chem.* **2008**, *29*, 1859–1865.

24. Huang, B.; Vetting, M.W.; Roderick, S.L. The Active Site of *O*-Acetylserine Sulfhydrylase Is the Anchor Point for Bienzyme Complex Formation with Serine Acetyltransferase. *J. Bacteriol.* **2005**, *187*, 3201–3205. [PubMed]
25. Phillips, J.C.; Hardy, D.J.; Maia, J.D.C.; Stone, J.E.; Ribeiro, J.V.; Bernardi, R.C.; Buch, R.; Fiorin, G.; Hénin, J.; Jiang, W. Scalable Molecular Dynamics on CPU and GPU Architectures with NAMD. *J. Chem. Phys.* **2020**, *153*, 044130. [CrossRef] [PubMed]
26. Zoete, V.; Cuendet, M.A.; Grosdidier, A.; Michielin, O. SwissParam: A Fast Force Field Generation Tool for Small Organic Molecules. *J. Comput. Chem.* **2011**, *32*, 2359–2368. [CrossRef] [PubMed]
27. Neese, F. The ORCA Program System. *Wiley Interdiscip. Rev. Comput. Mol. Sci.* **2012**, *2*, 73–78.
28. Hoagland, D.R.; Arnon, D.I. The Water-Culture Method for Growing Plants without Soil. *Calif. Agr. Expt. Sta. Circ.* **1950**, *347*, 1–32.
29. Randewig, D.; Hamisch, D.; Herschbach, C.; Eiblmeier, M.; Gehl, C.; Jurgeleit, J.; Skerra, J.; Mendel, R.R.; Rennenberg, H.; Hänsch, R. Sulfite Oxidase Controls Sulfur Metabolism under SO_2 Exposure in *Arabidopsis thaliana*. *Plant Cell Environ.* **2012**, *35*, 100–115. [CrossRef]
30. Machado, E.C.; Schmidt, P.T.; Medina, C.L.; Ribeiro, E.R.V. Photosynthetic Responses of Three Citrus Species to Environmental Factors. *Pesqui. Agropecu. Bras.* **2005**, *40*, 1161–1170. [CrossRef]
31. Moriwaki, T.; Falcioni, R.; Tanaka, F.A.O.; Cardoso, K.A.K.; Souza, L.A.; Benedito, E.; Nanni, M.R.; Bonato, C.M.; Antunes, W.C. Nitrogen-Improved Photosynthesis Quantum Yield Is Driven by Increased Thylakoid Density, Enhancing Green Light Absorption. *Plant Sci.* **2019**, *278*, 1–11. [CrossRef]
32. Genty, B.; Briantais, J.M.; Baker, N.R. The Relationship between the Quantum Yield of Photosynthetic Electron Transport and Quenching of Chlorophyll Fluorescence. *Biochim. Biophys. Acta-Gen. Subj.* **1989**, *990*, 87–92. [CrossRef]
33. Marchiosi, R.; de Souza Bido, G.; Böhm, P.A.F.; Soares, A.R.; da Silva, H.A.; Ferro, A.P.; de Lourdes Lucio Ferrarese, M.; Ferrarese-Filho, O. Photosynthetic Response of Soybean to L-DOPA and Aqueous Extracts of Velvet Bean. *Plant Growth Regul.* **2016**, *80*, 171–182. [CrossRef]
34. Malavolta, E.; Vitti, G.C.; Oliveira, S.A. *Avaliação Do Estado Nutricional Das Plantas: Princípios e Aplicações*; Potafos: Piracicaba, Brazil, 1997; p. 319.
35. Dayan, F.E.; Duke, S.O. Discovery for New Herbicide Sites of Action by Quantification of Plant Primary Metabolite and Enzyme Pools. *Engineering* **2020**, *6*, 509–514. [CrossRef]
36. Künstler, A.; Gullner, G.; Ádám, A.L.; Kolozsváriné Nagy, J.; Király, L. The Versatile Roles of Sulfur-Containing Biomolecules in Plant Defense—A Road to Disease Resistance. *Plants* **2020**, *9*, 1705.
37. Romero, L.C.; Aroca, M.Á.; Laureano-Marín, A.M.; Moreno, I.; García, I.; Gotor, C. Cysteine and Cysteine-Related Signaling Pathways in Arabidopsis Thaliana. *Mol. Plant* **2014**, *7*, 264–276. [CrossRef] [PubMed]
38. Martarello, D.C.I.; Grizza, L.H.E.; Foletto-Felipe, M.d.P.; Mendonça, A.P.d.S.; Constantin, R.P.; Ferro, A.P.; dos Santos, W.D.; Constantin, R.P.; Marchiosi, R.; Ferrarese-Filho, O. S-Benzyl-L-Cysteine Inhibits Growth and Photosynthesis, and Triggers Oxidative Stress in *Ipomoea grandifolia*. *Agronomy* **2024**, *14*, 1633. [CrossRef]
39. Lange, A.; Cavalli, E.; Pereira, C.S.; Chapla, M.V.; Da Silva Freddi, O. Calcium:Magnesium Ratio and Chemical Characteristics of Soil under Crop of Soy and Corn. *Nativa* **2021**, *9*, 294–301. [CrossRef]
40. Li, T.; Yan, A.; Bhatia, N.; Altinok, A.; Afik, E.; Durand-Smet, P.; Tarr, P.T.; Schroeder, J.I.; Heisler, M.G.; Meyerowitz, E.M. Calcium Signals Are Necessary to Establish Auxin Transporter Polarity in a Plant Stem Cell Niche. *Nat. Commun.* **2019**, *10*, 726. [CrossRef]
41. Farhat, N.; Elkhouni, A.; Zorrig, W.; Smaoui, A.; Abdelly, C.; Rabhi, M. Effects of Magnesium Deficiency on Photosynthesis and Carbohydrate Partitioning. *Acta Physiol. Plant.* **2016**, *38*, 145. [CrossRef]
42. Tian, X.Y.; He, D.D.; Bai, S.; Zeng, W.Z.; Wang, Z.; Wang, M.; Wu, L.Q.; Chen, Z.C. Physiological and Molecular Advances in Magnesium Nutrition of Plants. *Plant Soil* **2021**, *468*, 1–17. [CrossRef]
43. Lapaz, A.d.M.; Yoshida, C.H.P.; Gorni, P.H.; de Freitas-Silva, L.; Araújo, T.d.O.; Ribeiro, C. Iron Toxicity: Effects on the Plants and Detoxification Strategies. *Acta Bot. Bras.* **2022**, *36*, e2021abb0131. [CrossRef]
44. Wairich, A.; De Conti, L.; Lamb, T.I.; Keil, R.; Neves, L.O.; Brunetto, G.; Sperotto, R.A.; Ricachenevsky, F.K. Throwing Copper Around: How Plants Control Uptake, Distribution, and Accumulation of Copper. *Agronomy* **2022**, *12*, 994. [CrossRef]
45. Kaur, H.; Garg, N. Zinc Toxicity in Plants: A Review. *Planta* **2021**, *253*, 129. [CrossRef]
46. Alejandro, S.; Höller, S.; Meier, B.; Peiter, E. Manganese in Plants: From Acquisition to Subcellular Allocation. *Front. Plant Sci.* **2020**, *11*, 517877. [CrossRef]
47. Prusty, S.; Sahoo, R.K.; Nayak, S.; Poosapati, S.; Swain, D.M. Proteomic and Genomic Studies of Micronutrient Deficiency and Toxicity in Plants. *Plants* **2022**, *11*, 2424. [CrossRef]
48. Yang, M.; Jiao, Y. Regulation of Axillary Meristem Initiation by Transcription Factors and Plant Hormones. *Front. Plant Sci.* **2016**, *7*, 183. [CrossRef]
49. Taiz, L.; Zeiger, E.; Møller, I.M.; Murphy, A. *Fisiologia e Desenvolvimento Vegetal*, 6th ed.; Artmed: Porto Alegre, RS, Brazil, 2017; ISBN 9788582713679.

50. Su, Y.H.; Liu, Y.B.; Zhang, X.S. Auxin-Cytokinin Interaction Regulates Meristem Development. *Mol. Plant* **2011**, *4*, 616–625. [CrossRef]
51. Buchanan, B.B.; Gruissem, W.; Jones, R.L. *Biochemistry & Molecular Biology of Plants*; Wiley: Hoboken, NJ, USA, 2015; ISBN 9780470714218.

Disclaimer/Publisher's Note: The statements, opinions and data contained in all publications are solely those of the individual author(s) and contributor(s) and not of MDPI and/or the editor(s). MDPI and/or the editor(s) disclaim responsibility for any injury to people or property resulting from any ideas, methods, instructions or products referred to in the content.